

ORIGINAL RESEARCH

Acute Genetic Ablation of Cardiac Sodium/Calcium Exchange in Adult Mice: Implications for Cardiomyocyte Calcium Regulation, Cardioprotection, and Arrhythmia

Sabine Lotteau , PhD; Rui Zhang, MD; Adina Hazan, PhD; Christina Grabar, BS; Devina Gonzalez , BS; Stephan Aynaszyan, BS; Kenneth D. Philipson, PhD; Michela Ottolia, PhD; Joshua I. Goldhaber , MD

BACKGROUND: Sodium-calcium (Ca^{2+}) exchanger isoform 1 (NCX1) is the dominant Ca^{2+} efflux mechanism in cardiomyocytes and is critical to maintaining Ca^{2+} homeostasis during excitation-contraction coupling. NCX1 activity has been implicated in the pathogenesis of cardiovascular diseases, but a lack of specific NCX1 blockers complicates experimental interpretation. Our aim was to develop a tamoxifen-inducible NCX1 knockout (KO) mouse to investigate compensatory adaptations of acute ablation of NCX1 on excitation-contraction coupling and intracellular Ca^{2+} regulation, and to examine whether acute KO of NCX1 confers resistance to triggered arrhythmia and ischemia/reperfusion injury.

METHODS AND RESULTS: We used the α -myosin heavy chain promoter (Myh6)-MerCreMer promoter to create a tamoxifen-inducible cardiac-specific NCX1 KO mouse. Within 1 week of tamoxifen injection, NCX1 protein expression and current were dramatically reduced. Diastolic Ca^{2+} increased despite adaptive reductions in Ca^{2+} current and action potential duration and compensatory increases in excitation-contraction coupling gain, sarcoplasmic reticulum Ca^{2+} ATPase 2 and plasma membrane Ca^{2+} ATPase. As these adaptations progressed over 4 weeks, diastolic Ca^{2+} normalized and SR Ca^{2+} load increased. Left ventricular function remained normal, but mild fibrosis and hypertrophy developed. Transcriptomics revealed modification of cardiovascular-related gene networks including cell growth and fibrosis. NCX1 KO reduced spontaneous action potentials triggered by delayed afterdepolarizations and reduced scar size in response to ischemia/reperfusion.

CONCLUSIONS: Tamoxifen-inducible NCX1 KO mice adapt to acute genetic ablation of NCX1 by reducing Ca^{2+} influx, increasing alternative Ca^{2+} efflux pathways, and increasing excitation-contraction coupling gain to maintain contractility at the cost of mild Ca^{2+} -activated hypertrophy and fibrosis and decreased survival. Nevertheless, KO myocytes are protected against spontaneous action potentials and ischemia/reperfusion injury.

Key Words: arrhythmia ■ calcium transients ■ excitation-contraction coupling ■ ischemia/reperfusion ■ knock out mice ■ sodium-calcium exchange

See Editorial by Bers and Nattel

Cardiac excitation-contraction (EC) coupling is the process whereby electrical excitation of the cell membrane produces contraction of the

myocyte. Action potentials (APs) depolarize the sarcolemma and activate voltage-dependent L-type calcium (Ca^{2+}) channels (LCCs) in the transverse tubules,

Correspondence to: Joshua I. Goldhaber, MD, Smidt Heart Institute, Cedars-Sinai Medical Center, 8700 Beverly Boulevard, Los Angeles, CA 90048. E-mail: joshua.goldhaber@cshs.org

Supplementary Material for this article is available at <https://www.ahajournals.org/doi/suppl/10.1161/JAHA.120.019273>

For Sources of Funding and Disclosures, see page 18.

© 2021 The Authors. Published on behalf of the American Heart Association, Inc., by Wiley. This is an open access article under the terms of the Creative Commons Attribution-NonCommercial-NoDerivs License, which permits use and distribution in any medium, provided the original work is properly cited, the use is non-commercial and no modifications or adaptations are made.

JAHA is available at: www.ahajournals.org/journal/jaha

CLINICAL PERSPECTIVE

What Is New?

- We created a tamoxifen-inducible cardiac-specific sodium-calcium exchanger isoform 1 (NCX1) knockout mouse, which effectively eliminates NCX1 in adult mouse heart without reducing ventricular function.
- The tamoxifen-inducible knockout approach facilitates study of critical time-dependent adaptations of excitation-contraction coupling and intracellular calcium regulation in response to acute NCX1 ablation, which allow these mice to survive up to 5 months.
- Transcriptomics demonstrate cardiovascular and other gene network changes in response to NCX1 ablation, with increased fibrotic networks identified by 4 weeks postablation; acute genetic ablation of NCX1 protects against ischemia/reperfusion injury and suppresses arrhythmogenic delayed afterdepolarizations.

What Are the Clinical Implications?

- Blocking NCX1 is a potential therapeutic approach to reduce ischemia/reperfusion injury and triggered arrhythmia in the heart.
- The tamoxifen-inducible NCX1 knockout mouse can be used as a simple tool to test this strategy in mouse models of human disease through cross-breeding, with confidence that ablation of NCX1 is specific and complete.
- This mouse can also be used to test the pharmacological specificity of new NCX1 blockers, many of which are known to have off-target effects.

Nonstandard Abbreviations and Acronyms

AM	acetoxymethyl ester
AP	action potential
APD	action potential duration
Ca²⁺	calcium
CaMKII	calcium/calmodulin-dependent protein kinase II
Cre	Cre recombinase
DAD	delayed after depolarization
EC	excitation-contraction
I_{Ca}	calcium current
I_{NCX}	sodium-calcium exchanger current
I_{NCX1}	sodium-calcium exchanger isoform 1 current
IPA	Ingenuity Pathway Analysis
I_{to}	transient outward potassium current

KO	knockout
LCC	L-type calcium channel
MLC2v	ventricular myosin light chain-2
NCX	sodium-calcium exchanger
NCX1	sodium-calcium exchanger isoform 1
NCX1F_x/F_x	sodium-calcium exchanger isoform 1 exon 11 floxed mice
PGC-1α	peroxisome proliferator-activated receptor γ coactivator 1 α
PMCA	plasma membrane calcium ATPase
RyR	ryanodine receptor
sAP	spontaneous action potential
SERCA2	sarcoplasmic reticulum calcium ATPase 2
SR	sarcoplasmic reticulum

allowing Ca²⁺ to enter the restricted space known as the dyadic cleft. This Ca²⁺ then triggers ryanodine receptors (RyRs) on the sarcoplasmic reticulum (SR) to open and release Ca²⁺ into the cytosol, where it binds to myofilaments and induces contraction of the myocyte. Upon repolarization, relaxation occurs when most of the Ca²⁺ is removed from the cytoplasm and pumped back into the SR by the SR Ca²⁺ ATPase 2 (SERCA2). The remaining Ca²⁺ is extruded from the cytoplasm by the sodium (Na⁺)-Ca²⁺ exchanger (NCX) isoform 1 (NCX1), although a small proportion is also removed by the plasma membrane Ca²⁺ ATPase (PMCA) and the mitochondrial Ca²⁺ uniporter.^{1,2} NCX1 is considered essential for maintaining Ca²⁺ balance, extruding almost the precise amount of Ca²⁺ that enters the cell through LCCs.³ NCX1 is also electrogenic. Under physiological conditions, NCX1 transports 3 Na⁺ into and 1 Ca²⁺ out of the cell, generating an inward current.^{2,4} In addition to its essential role in the inotropic effect of cardiac glycosides,⁵ NCX1 has been implicated in the pathogenesis of several different cardiovascular diseases such as heart failure with reduced ejection fraction, ischemia/reperfusion (I/R) injury, and arrhythmias.⁶

Several NCX inhibitors, notably KB-R7943, SEA0400, ORM-10103, and ORM-10962, have been developed to both study the role of NCX in the heart and also to assess the potential of NCX inhibition as a disease therapy. However, the specificity of these agents is either known to be incomplete or not well established,⁷⁻¹⁰ which complicates interpretation of results. In contrast, genetic knockout (KO) models are specific for the target gene but pose different challenges. For example, global KO of NCX1 is embryonic lethal, possibly because of vascular rarefaction during embryogenesis.^{5,11-13} Our prior ventricular-specific Cre recombinase (Cre)/lox KO

of NCX1, where Cre expression is under the control of the endogenous ventricular myosin light chain-2 (MLC2v) promoter,¹⁴ lives into adulthood with NCX1 totally eliminated in $\approx 90\%$ of cardiomyocytes. Adaptations of EC coupling and Ca regulation that allow these mice to survive without NCX have informed the field about the plasticity of EC coupling systems and their range of compensation. While these mice have provided invaluable data, their utility is compromised by modest reduction in ejection fraction, increased ventricular hypertrophy and fibrosis, and reduced survival.¹⁴⁻¹⁷ In addition, their shortened lifespan makes them difficult to breed or study at older ages.

To address these concerns, we created a tamoxifen-inducible cardiac-specific NCX1 KO mouse. These mice make it possible, for the first time, to assess in adult mice the temporal effects of acute NCX1 ablation on cardiac function, EC coupling, and Ca²⁺ regulation by the simple application of tamoxifen. In addition to evaluating the time course and nature of EC coupling adaptations, we exploited next-generation RNA sequencing to better understand the progression of adaptive gene expression

in these animals over a 4-week period. To compare with our previous NCX1 KO models, we tested the efficacy of these mice at reducing arrhythmogenic spontaneous APs (sAPs) and I/R injury. We found that tamoxifen-inducible NCX1 KO mice survive acute genetic ablation of NCX1 by a different set of adaptive Ca²⁺-handling mechanisms than we previously observed in our MLC2v chronic ablation model. Furthermore, the tamoxifen model maintains normal left ventricular (LV) function, has far less fibrosis than the MLC2v NCX1 KO mouse, and retains protection against I/R and arrhythmogenic sAPs.

METHODS

This study was approved by the Cedars-Sinai Institutional Animal Care and Use Committee and adhered to the *Guide for the Care and Use of Laboratory Animals* prepared by the Committee for the Update of the Guide for the Care and Use of Laboratory Animals of the Institute of Laboratory Animal Research, National Research Council. The data that support the findings of this study are available from the corresponding author upon reasonable request.

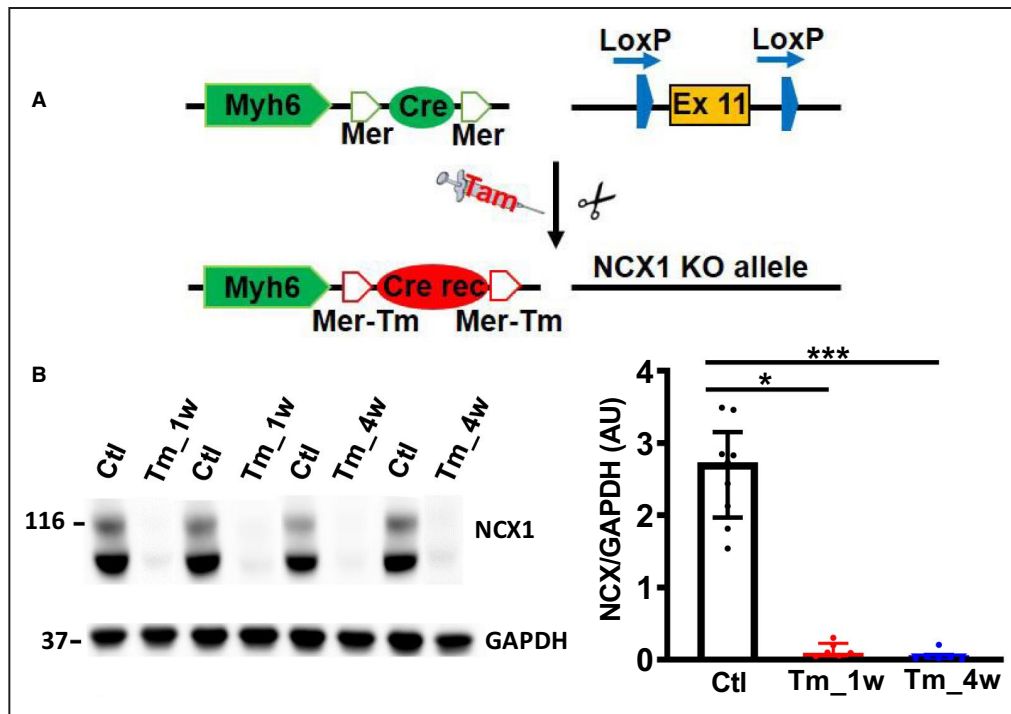


Figure 1. Generation of sodium-calcium exchanger (NCX) isoform 1 (NCX1) knockout (KO) mice. **A**, NCX1 floxed mice (exon 11 of the NCX1 gene *Slc8a1* flanked by loxP sites) were crossed with α -myosin heavy chain promoter (*Myh6*) (α MHC)-MerCreMer mice to obtain NCX1 exon 11 floxed mice (NCX1^{Fx}/MerCreMer) mice under control of the α -MHC promoter. **B**, Representative Western blots (left) and mean data normalized to GAPDH (right) showing NCX1 (116 and 70 kDa) expression in the ventricle of control mice (Ctl, black) and tamoxifen-inducible NCX1 KO mice at 1 week (Tm_1w, red) and 4 weeks (Tm_4w, blue) after tamoxifen injection (40 mg/kg during 5 consecutive days). Control mice received peanut oil injection as placebo. Data are expressed as median and interquartile range. Cre rec indicates Cre recombinase. * $P < 0.05$, *** $P < 0.001$ by Kruskal-Wallis test.

Cardiac-Specific KO of NCX1

Mice studies were conducted in accordance with the National Institutes of Health *Guide for the Care and Use of Laboratory Animals*. To produce tamoxifen-inducible NCX1 KO mice (Figure 1A), we crossed our previously described NCX1 exon 11 floxed mice (NCX1^{Fx/Fx})¹⁴ with α -myosin heavy chain promoter (Myh6)-MerCreMer transgenic mice (The Jackson Laboratory, mouse strain 005657) on a C57BL/6 background as described,^{18,19} allowing the creation of NCX1^{Fx/Fx}/MerCreMer mice. To ablate NCX1 in these mice, 4-hydroxytamoxifen (tamoxifen) diluted into peanut oil (40 mg/kg) was injected daily intraperitoneal for 5 consecutive days (we refer to these mice hereafter as NCX1 KO mice). Control mice received peanut oil injection without tamoxifen. Male and female mice, aged 9 to 12 weeks, were used for experiments.

Echocardiography

Mice were anesthetized with 3% isoflurane (induction) and maintained with 1.5% isoflurane on a heated platform for transthoracic echocardiography (Vevo 3100, VisualSonics). Systolic function (ejection fraction and LV fractional shortening), chamber dimensions, and wall thickness were evaluated using an average of 3 M-mode images obtained in the parasternal short-axis view at the level of the papillary muscles. Echocardiography was performed on 17 control mice, 16 mice 1 week post-tamoxifen injection, and 12 mice 4 weeks post-tamoxifen injection.

Protein Biochemistry

Mouse ventricle heart homogenate (10–20 μ g) was dissolved in sodium dodecyl sulfate–reducing buffer. Proteins were separated on 4% to 12% SDS-PAGE and transferred to nitrocellulose membrane. Blots were probed with antibodies specific for Ca_v1.2 (Alomone ACC 003, 1:600; Alomone Labs), SERCA2 (Thermo Fisher MA3 919, 1:1000; Thermo Fisher Scientific), Phospholamban (Thermo Fisher PA5 78410, 1:1000; Thermo Fisher Scientific), NCX1 (Swant R3F1, Swant), PMCA4 (Thermo Fisher MA1 914, 1:1000; Thermo Fisher Scientific), CaMKII (Abcam 52476, 1:1000; Abcam), Phospho-CaMKII (Abcam 32678, 1:1000; Abcam), K_v4.2 (Sigma P0233, 1:500; Sigma-Aldrich), and GAPDH (Sigma G9545, 1:10 000; Sigma-Aldrich). Immunoreactivity was detected by chemiluminescence (SuperSignal West Pico Plus, Thermo Fisher Scientific) using a ChemiDoc Imager (BioRad). Multiple bands for Ca²⁺/calmodulin-dependent protein kinase II (CaMKII), phosphorylated CaMKII (p-CaMKII), and Kv4.2 were analyzed together to avoid bias. Protein biochemistry was performed on 9 control mice, 6 mice 1 week

post-tamoxifen injection, and 6 mice 4 weeks post-tamoxifen injection.

Masson Trichrome Staining

Midventricular heart tissues were embedded in paraffin and sectioned by the Cedars-Sinai Biobank and Translational Research core with staining performed by the Cedars-Sinai Clinical Histology laboratory. Myocardial fibrosis (blue-gray pixels divided by total pixels) was quantified using ImageJ software (version 1.48v²⁰). Masson trichrome staining was performed on 7 control mice, 3 mice 1 week post-tamoxifen injection, and 5 mice 4 weeks post-tamoxifen injection.

Next-Generation RNA Sequencing

We isolated total RNA from ventricular heart tissue using the RNeasy Kit (Qiagen). Libraries for RNA sequencing were prepared with KAPA RNA HyperPrep Kit with RiboErase (KAPA Biosystem). A total of 1000 ng RNA was used as input. Sequencing was performed by the UCLA Technology Center for Genomics & Bioinformatics on an Illumina HiSeq 3000 (Illumina, Inc.) for a single read of 50 runs. A data quality check was performed on an Illumina Sequencing Analysis Viewer. Demultiplexing was performed with Illumina Bcl2fastq2 Conversion Software (v2.17). Differentially expressed genes were identified using edgeR software.²¹ Genes showing altered expression with $P < 0.05$ and > 1.5 -fold changes were considered differentially expressed. The pathway and network analyses were performed using Ingenuity Pathway Analysis (IPA) software (Qiagen) using settings specific to mouse and heart. Next-generation RNA sequencing was performed on 3 control mice, 3 mice 1 week post-tamoxifen injection, and 3 mice 4 weeks post-tamoxifen injection.

Isolation of Cardiomyocytes

Adult ventricular cardiomyocytes were isolated as described.¹⁴ In brief, heparin (4000 IU/kg) was intraperitoneally injected 30 minutes before excising the heart. Each mouse was euthanized under 5% isoflurane. The heart was quickly removed by thoracotomy; rinsed in Ca²⁺-free Tyrode solution containing (in mmol/L): 136 NaCl, 5.4 KCl, 0.33 NaH₂PO₄, 1.0 MgCl₂, 10 HEPES, and 10 glucose (pH adjusted to 7.4); and mounted on a Langendorff apparatus for retrograde aortic perfusion. Each heart was perfused at 3 mL/min at 37°C with Ca²⁺-free Tyrode solution for 5 minutes, then 12 minutes with Ca²⁺-free Tyrode solution containing type II collagenase (1 mg/mL, Worthington Biomedical) and type XIV protease (0.13 mg/mL, Sigma-Aldrich).

After enzymatic digestion, the heart was perfused with Tyrode solution containing 0.2 mmol/L CaCl_2 for 5 minutes. Single cells were then manually dissociated by trituration using forceps and filtered (100 μm). Ca^{2+} was gradually reintroduced to a final concentration of 1 mmol/L. We stored isolated cardiomyocytes for up to 6 hours at room temperature (20°C–22°C).

Single-Cell Electrophysiology and Ca^{2+} Transients

Isolated cardiomyocytes were placed in a flow-through optical chamber on the stage of an inverted microscope. The chamber was constantly perfused with control Tyrode or experimental solutions as detailed below (at 20°C–22°C). For voltage clamp experiments, we recorded membrane current using the whole cell patch clamp technique and an Axopatch 200B amplifier (Molecular Devices) connected to a computer by a Digidata 1400a A-D converter (Molecular Devices) controlled by pClamp software (version 10.4; Molecular Devices). For current clamp experiments, we recorded membrane voltage in patch-clamped myocytes using the bridge balance mode of an Axoclamp 900A amplifier. Patch electrodes were pulled from borosilicate glass (TW150F-3, World Precision Instruments) using a Flaming-Brown horizontal micropipette puller (P-97, Sutter Instruments). Pipettes had an electrical resistance of 0.75 to 2 M Ω for voltage clamp and 0.9 to 1.5 M Ω for current clamp.

In some experiments we simultaneously recorded membrane current and intracellular Ca^{2+} in myocytes loaded with Fluo-4 acetoxymethyl ester (AM) using a custom-built photometric epifluorescence detection system attached to a Zeiss Axiovert TV100 inverted microscope (Carl Zeiss Microscopy) fitted with a 40 \times water immersion objective (C-Apochromat 40/1.2 W Corr; Zeiss). A 485-nm LED light source provided excitation and we used a long pass filter to restrict emission to >510 nm. The emission fluorescence was recorded using an avalanche photodiode (Hamamatsu C5460) passed through a 100-KHz analog filter and then inverted. Fluorescence ratios were normalized to baseline (F/F_0) after background subtraction. We loaded cells with Fluo-4 AM (5 $\mu\text{mol/L}$ with 0.02% Pluronic F-127 dissolved in the 1 mmol/L Ca^{2+} Tyrode solution described above for cell isolation, 20 minutes loading at room temperature followed by 3 washes in Tyrode solution).

For patch clamp recordings of NCX1 current (I_{NCX1}) and calcium current (I_{Ca}) in Fluo-4 AM-loaded cells, the bath solution contained (in mmol/L): 136 NaCl, 20 CsCl, 1 MgCl_2 , 10 HEPES, 10 glucose, 1 CaCl_2 , and 0.01 tetrodotoxin (pH adjusted to 7.4 NaOH). The

internal solution contained (in mmol/L): 110 CsCl, 10 NaCl, 0.33 MgCl_2 , 30 tetraethylammonium chloride, 10 HEPES, 0.05 cAMP, and 5 MgATP (pH adjusted to 7.2 with CsOH). To measure APs using the bridge balance current clamp mode of the Axoclamp 900A, cells were placed in the 1-mmol/L Ca^{2+} Tyrode solution described above. Internal solution contained (in mmol/L): 110 KCl, 10 NaCl, 1 MgCl_2 , 10 HEPES, 5 Phosphocreatine, 5 MgATP, 0.05 cAMP (pH adjusted to 7.2 with KOH). To measure transient outward potassium current (I_{to}) using the Axopatch 200B, the bath solution contained (in mmol/L): 136 NaCl, 5.4 KCl, 10 HEPES, 1 MgCl_2 , 0.33 NaH_2PO_4 , 1 CaCl_2 , 10 glucose, 0.01 tetrodotoxin, and 0.002 nifedipine (pH adjusted to 7.4 NaOH), while the internal solution contained (in mmol/L): 130 KCl, 1 MgCl_2 , 5.4 NaCl, 10 HEPES, 5 MgATP, 0.05 cAMP, and 2.8 phosphocreatine (pH adjusted to 7.2 with KOH). Single-cell electrophysiology and Ca^{2+} transients were performed on 5 control mice, 4 mice 1 week post-tamoxifen injection, and 3 mice 4 weeks post-tamoxifen injection.

Measurements of Cytosolic Ca^{2+} Using Fura-2

To record Ca^{2+} transients with field stimulation, we loaded cardiomyocytes with Fura-2 AM (2.5 $\mu\text{mol/L}$ for 20 minutes dissolved in the 1-mmol/L Ca^{2+} Tyrode solution and 0.02% Pluronic F-127 at room temperature) and placed them in a flow-through optical chamber with integrated platinum pacing electrodes (RC-27, Warner Instruments). The chamber was placed on an inverted microscope (Leica DMI3000 B) fitted with a 40 \times /1.2NA oil immersion lens and attached to a custom-built high-speed dual excitation/single-emission epifluorescence system. Cells were alternately excited (at 500 Hz) by 360 and 390 nm light-emitting diodes. Emission fluorescence was collected at 510 nm using a photomultiplier (IonOptix) and digitized using the Digidata A-D converter. Cells were field-stimulated at 1 Hz using a MyoPacer Field Stimulator (IonOptix) at 30 volts for 10 seconds to equilibrate SR Ca^{2+} content, and then we recorded the fluorescence signal for 20 seconds during continued pacing. After background subtraction, we calculated the F360/F390 ratio. Given the inherent errors involved with Fura-2 calibration^{22,23} and the high reproducibility of uncalibrated Fura-2 fluorescence ratios, we chose to report the latter. Control and tamoxifen samples were always studied during the same week to negate any potential drift in the instrument (which nevertheless we did not detect). Cytosolic Ca^{2+} measurements using Fura-2 were performed on 8 control mice, 4 mice 1 week post-tamoxifen injection, and 6 mice 4 weeks post-tamoxifen injection.

Assessment of Ca²⁺ Waves Using Confocal Microscopy

Confocal images of isolated ventricular myocytes were acquired using a Leica TCS SP5 II microscope (Leica Microsystems Inc.) with a 63×/1.2 water immersion objective lens. We loaded myocytes with 5 μmol/L Fluo-4 AM (Thermo Fisher Scientific) and 0.02% Pluronic F-127 (ThermoFisher) at 20°C for 20 minutes, followed by three 15-minute washing periods. The cell suspension was then placed in an experimental flow-through chamber with a coverslip bottom on the inverted stand of the microscope. We used the 488-nm excitation line of the argon laser and recorded emission >510 nm, with line scan (xt) mode at 400 lines per second. Cells were paced for 5 beats at 1 Hz (10 mV, pulse width 3 ms) to equilibrate SR Ca²⁺. We imaged the last 2 stimulations before field stimulation was stopped, and then continued recording to capture spontaneous waves. Ca²⁺ waves were analyzed by counting the total number of waves during the 10.8-second recording period and are reported as waves per second. We calculated velocity from the slope of the wave on the line scan. Ca²⁺ wave measurements were performed on 8 control mice, 4 mice 1 week post-tamoxifen injection, and 6 mice 4 weeks post-tamoxifen injection.

Ischemia/Reperfusion

Hearts were quickly removed from anesthetized mice and then mounted on a Langendorff apparatus and perfused with Tyrode solution containing (in mmol/L): 136 NaCl, 5.4 KCl, 0.33 NaH₂PO₄, 1.0 MgCl₂, 10 HEPES, 1.8 CaCl₂, and 10 glucose (pH adjusted to 7.4 NaOH) 3 mL/min for 20 minutes at 37°C. Hearts were then subjected to 20 minutes zero-flow (ischemia) followed by 120 minutes of reperfusion. After reperfusion, hearts were cut at a thickness of 1 mm, stained with 1% 2,3,5-triphenyltetrazolium chloride dissolved in Tyrode solution at 37°C for 30 minutes, and fixed in formalin.²⁴ Necrosis area was determined by measuring the stained red area (live tissue) versus the unstained white area (necrotic) using ImageJ software and manual tracing, expressed as a percentage of the total slice area.²⁵ I/R experiments were performed on 8 control mice, 3 mice 1 week post-tamoxifen injection, and 6 mice 4 weeks post-tamoxifen injection.

Statistical Analysis

Results are expressed as mean±SEM (Student *t* test, 1-way ANOVA) or as median and interquartile range (Mann-Whitney and Kruskal-Wallis tests). Differences are considered significant when *P*<0.05. The Shapiro-Wilk statistic was used to test for normality. Comparison of 2 groups was performed using

Student *t* test (normal distribution) and Mann-Whitney rank test (non-normal distribution). Comparisons of 3 groups were performed with 1-way ANOVA (normal distribution) with Tukey test for post hoc analysis or Kruskal-Wallis test (non-normal distribution) with Dunn test for post hoc analysis. The Kaplan-Meier plot was used to estimate the survival of the mice after tamoxifen injection. GraphPad Prism (version 8.01; Graphpad) was used for all statistical analysis. There were no repeated measurements on the same experimental unit. None of the 1-week post-tamoxifen mice were used later as 4-week post-tamoxifen mice.

RESULTS

Cardiac Function, Morphometrics, and Survival of Tamoxifen-Inducible NCX1 KO Mice

We first assessed the efficacy of NCX1 ablation at 1 and 4 weeks after injection of tamoxifen. At 1 week, the NCX1 protein in the ventricle was reduced by 95% (control 2.59±0.23 AU [N=9] and 1 week 0.13±0.04 AU [N=6]; *P*=0.0325) and by 4 weeks, the NCX1 protein was reduced by 98% (0.05±0.03 AU [N=6], *P*<0.001) (Figure 1B). One week after tamoxifen injection, there was no change in heart weight/body weight ratio, no change in LV systolic function as assessed by echocardiography (Table S1), and no cardiac fibrosis or cellular hypertrophy (Figure 2A through 2C). However, 4 weeks after tamoxifen injection, there was mild LV and cellular hypertrophy (heart weight/body weight ratio: control 6.6±0.1 mg/g [N=25] and 4 weeks 7.9±0.3 mg/g [N=13] [*P*<0.001]; myocyte cross-sectional area: control 215±8 μm² and 4 weeks 266±14 μm² [N=5] [*P*<0.001]) and an increase of fibrosis (control 1.1%±0.2% [N=7] and 4 weeks 5.8%±0.9% [N=5] [*P*<0.001]). Mice began dying 5 weeks after tamoxifen injection, and only 1 of 10 animals survived to 5 months after tamoxifen injection (Figure 2D). To ensure there was no tamoxifen toxicity, we injected either tamoxifen (40 mg/kg per day during 5 consecutive days) or peanut oil vehicle as the control in wild-type C57bl/6 mice. We observed no changes in heart weight/body weight ratio, fibrosis, or hypertrophy (Figure S1), and no increase in mortality.

Transcriptomics

Identification of Time-Dependent Gene Fold Changes

Next, we examined the time course of transcriptomic changes in NCX1 KO mice using next-generation RNA sequencing.^{26,27} A total of 16 871 (1 week

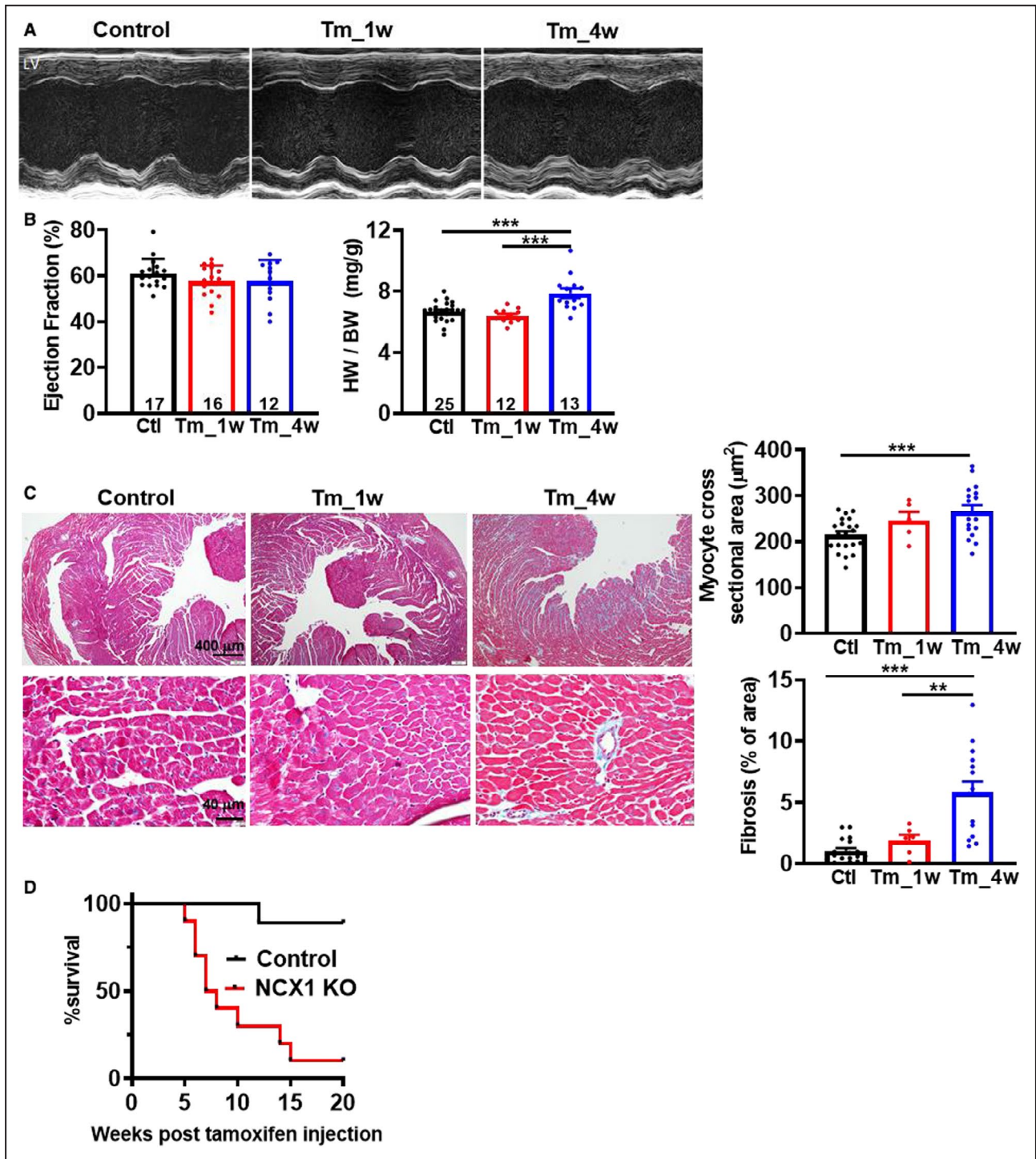


Figure 2. Cardiac function and morphometrics in tamoxifen-inducible sodium-calcium exchanger isoform 1 (NCX1) knockout (KO) mice.

A, Representative M-mode echocardiography of the left ventricle (parasternal short axis) in control mice (Ctl) and mice 1 week (Tm_1w) and 4 weeks (Tm_4w) post-tamoxifen. **B**, Summary data including left ventricular ejection fraction (percentage) and heart weight to body weight (HW/BW) ratio in Ctl and tamoxifen-inducible NCX1 KO mice at 1 week (Tm_1w) and 4 weeks (Tm_4w) post-tamoxifen injection. **C**, Masson trichrome staining of transverse heart sections and mean data showing myocyte cross-section area (μm^2) and fibrosis (percentage of total area) in control mice (Ctl, N=7) and tamoxifen-inducible NCX1 KO mice at 1 week (Tm_1w, N=3) and 4 weeks (Tm_4w, N=5) post-tamoxifen injection. **D**, Kaplan-Meier curve showing the percentage of survival post-tamoxifen injection. N=9 control and N=10 tamoxifen-treated NCX1 KO mice. Data are expressed as mean \pm SEM. ** P <0.01, *** P <0.001 by 1-way ANOVA.

post-tamoxifen versus control) and 17 137 (4 weeks post-tamoxifen versus control) transcripts were tested (N=3 mice per group). A fold change of ≥ 1.5 was used as a cutoff, with a P value of 0.05. At 1 week post-tamoxifen, a total of 182 gene transcripts were either upregulated (122) or downregulated (60) >1.5 -fold, of which 172 were mapped by IPA software. By 4 weeks post-tamoxifen, a total of 2699 gene transcripts were identified, either upregulated (1789) or downregulated (910), and 2554 were mapped by IPA (Figure 3A and 3B).

Network Analysis

IPA software enables systemic analysis in a biological context. Our upregulated or downregulated genes at the 2 time points (1 and 4 weeks after tamoxifen injection) were overlaid with a global molecular network developed in the IPA knowledge base. Networks of these genes were algorithmically generated based on their interrelationships. Using this approach, the software identified 5 major networks impacted 1 week after tamoxifen injection and 25 networks impacted 4 weeks after tamoxifen (Figure 3C and 3D and Table S2). At 1 week, the top-scoring cardiovascular network included genes with functions related to cardiac enlargement, cardiovascular disease, and cardiovascular system development and function. Examples of upregulated cardiac-related genes included MYC and peroxisome proliferative activated receptor γ coactivator 1 α (PPARGC1A) (Figure 3E). Four weeks post-tamoxifen injection, the top cardiovascular networks involved cardiac fibrosis, cardiovascular disease, and organismal injury, and involved upregulated genes such as transforming growth factor $\beta 3$ (TGF $\beta 3$), mitogen-activated protein kinase 11 (MAPK11), collagen type I $\alpha 1$ chain (COL1A1), collagen type III $\alpha 1$ chain (COL3A1), and caveolin 3 (CAV3), and downregulated genes such as phospholamban, calcium voltage-gated channel subunit $\alpha 1 C$ (CACNA1C), and Ca²⁺/calmodulin-dependent protein kinase II (CAMK2A) (Figure 3F).

NCX1 Function in Tamoxifen-Inducible NCX1 KO Mice

Having confirmed at the protein level that NCX1 was ablated, we next examined I_{NCX1} in patch-clamped enzymatically isolated ventricular myocytes loaded with the Ca²⁺-sensitive indicator Fluo-4 AM. To elicit NCX current (I_{NCX}), we rapidly applied 10 mmol/L of caffeine to the bath solution surrounding the cell using a rapid solution exchanger²⁸ while recording membrane current and Fluo-4 fluorescence (Figure 4A, V_H -70 mV). Each application of caffeine was preceded

by a conditioning train of five 100-ms prepulses from -40 to 0 mV at 1 Hz to ensure steady-state SR Ca²⁺ loading.^{16,29,30} Peak I_{NCX} was reduced by 74% and 87%, respectively, at 1 and 4 weeks post-tamoxifen injection (Figure 4A and 4B; control -1.42 ± 0.05 pA/pF [N=23], 1 week -0.37 ± 0.05 pA/pF [N=17] [$P < 0.001$], and 4 weeks -0.19 ± 0.05 pA/pF [N=19] [$P < 0.001$]). While I_{NCX1} was reduced in every cell at 1 and 4 weeks after tamoxifen injection, I_{NCX1} was completely eliminated in 25% of cells at 4 weeks (Figure 4B). The amplitude of the caffeine-induced Ca²⁺ transient, an indicator of SR Ca²⁺ load, was similar between control and 1 week post-tamoxifen, and modestly increased at 4 weeks post-tamoxifen injection (Figure 4C; control 3.03 ± 0.18 $\Delta F/F_0$ [N=26], 1 week 3.00 ± 0.19 $\Delta F/F_0$ [N=17], and 4 weeks 3.90 ± 0.36 $\Delta F/F_0$ [N=12] [$P = 0.0346$]). During sustained caffeine perfusion, we observed a decrease in the slope of the plateau of the Ca²⁺ transient at 1 and 4 weeks post-tamoxifen injection (Figure 4D), consistent with reduced Ca²⁺ efflux rate caused by NCX1 ablation.

EC Coupling in Tamoxifen-Inducible NCX1 KO Mice

In the same cells, we measured I_{Ca} and simultaneous Fluo-4 Ca²⁺ transients during 200 ms voltage clamps from -50 to +0 mV (Figure 5). We observed a 37% decrease of the peak amplitude of I_{Ca} 1 week post-tamoxifen and a 43% decrease at 4 weeks (Figure 5B; control -7.42 ± 0.40 pA/pF [N=25], 1 week -4.65 ± 0.46 pA/pF [N=17] [$P < 0.001$], 4 weeks -4.21 ± 0.33 pA/pF [N=12] [$P < 0.001$]). However, the decrease of I_{Ca} did not reduce the amplitude of the Ca²⁺ transient, indicating an increase in EC coupling gain in the NCX1 KO mice (Figure 5D). Furthermore, we observed no change in the relaxation half-time of the Ca²⁺ transient, consistent with the dominance of SR Ca²⁺ uptake in diastole (Figure 5E). We also noted a significant reduction in the transient inward current upon repolarization, a further indication of NCX ablation (Figure S2).

Since immunoblotting showed no decrease in Ca_v1.2 (calcium channel voltage-dependent L type $\alpha 1 C$ subunit) protein (Figure 6C), we hypothesized that reduction in I_{Ca} was related to Ca²⁺-dependent inactivation from elevated cytosolic or subsarcolemmal Ca²⁺. To test this hypothesis 1 week post-tamoxifen, we measured I_{Ca} in the presence and absence of the Ca²⁺ buffer EGTA (10 mmol/L) in the patch pipette solution. We found that EGTA eliminated the relative reduction in I_{Ca} observed in the NCX1 KO mouse (Figure 5C), consistent with Ca²⁺-dependent inactivation being the cause, and similar to what we observed in the MLC2v NCX1 KO mouse. In the latter case, Ca²⁺ transients were not obviously increased, so we inferred that elevated

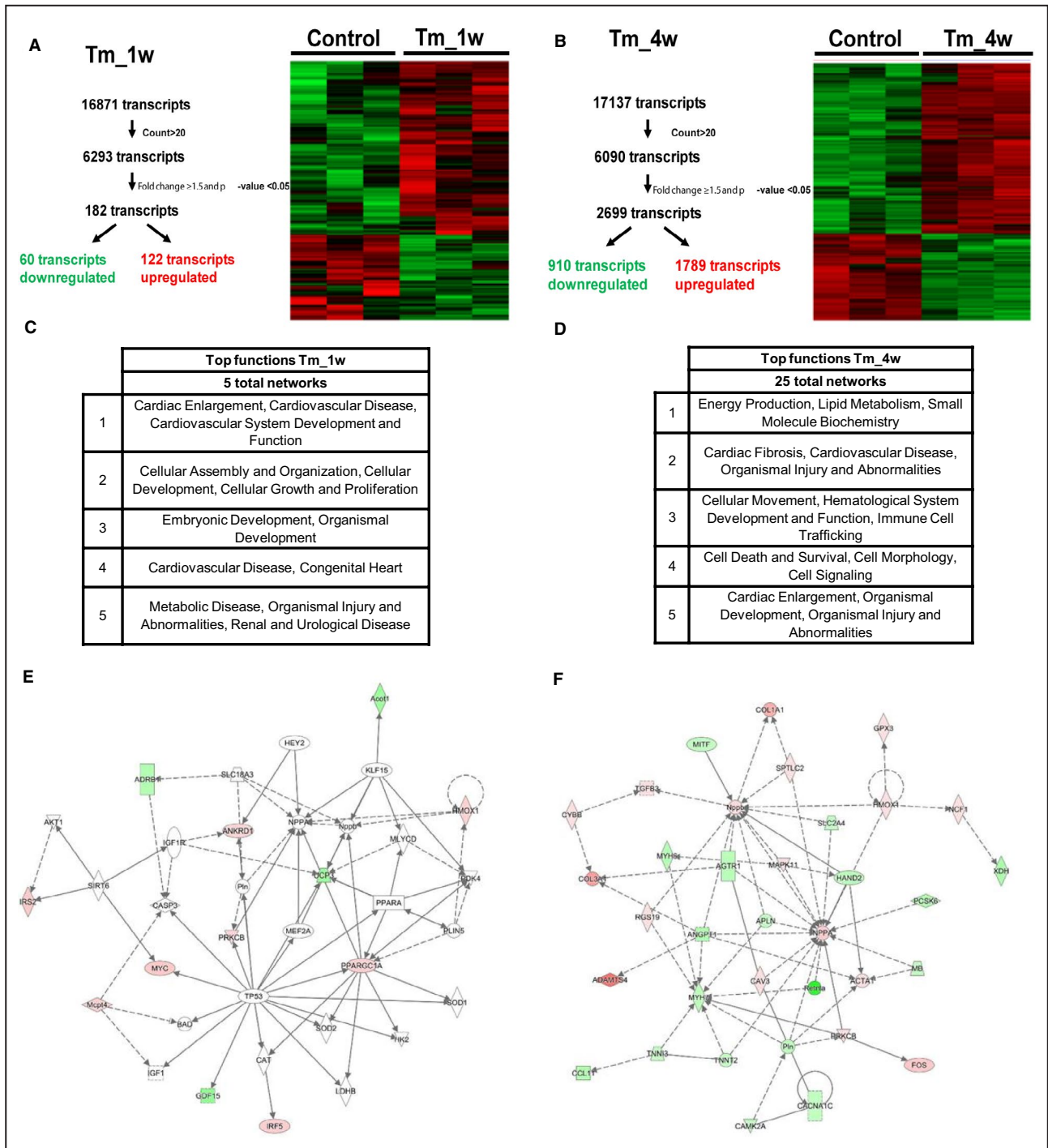


Figure 3. Transcriptomic changes in tamoxifen-inducible sodium-calcium exchanger isoform 1 (NCX1) knockout (KO) mice. **A**, Flowchart of RNA sequencing (left), heatmap of upregulated and downregulated transcripts (right) identified by Ingenuity Pathway Analysis (IPA) software associated with target genes from ventricles taken from control mice (N=3) vs tamoxifen 1 week (Tm_1w, N=3) and **(B)** 4 weeks (Tm_4w, N=3) post-tamoxifen injection. Threshold criteria: count >20, fold change ≥1.5, and P<0.05. **C**, Five major networks identified 1 week after tamoxifen injection (Tm_1w). **D**, Top 5 of 25 major networks identified 4 weeks after tamoxifen injection (Tm_4w). **E**, Top scoring network identified 1 week after tamoxifen injection, featuring genes related to cardiac enlargement, cardiovascular disease, and cardiovascular system development and function. These were mostly upregulated genes such as MYC and peroxisome proliferative activated receptor γ coactivator 1 α (PPARGC1A). **F**, Top cardiovascular network 4 weeks after tamoxifen injection, featuring genes with functions related to cardiac fibrosis, cardiovascular disease, and organismal injury and abnormalities. This network contained upregulated genes such as transforming growth factor β 3 (TGFB3), mitogen-activated protein kinase 11 (MAPK11), collagen type I α 1 chain (COL1A1), collagen type III α 1 chain (COL3A1), and caveolin 3 (CAV3), and downregulated genes such as phospholamban (Pln), calcium voltage-gated channel subunit α 1 C (CACNA1C), and calcium/calmodulin-dependent protein kinase II (CAMK2A).

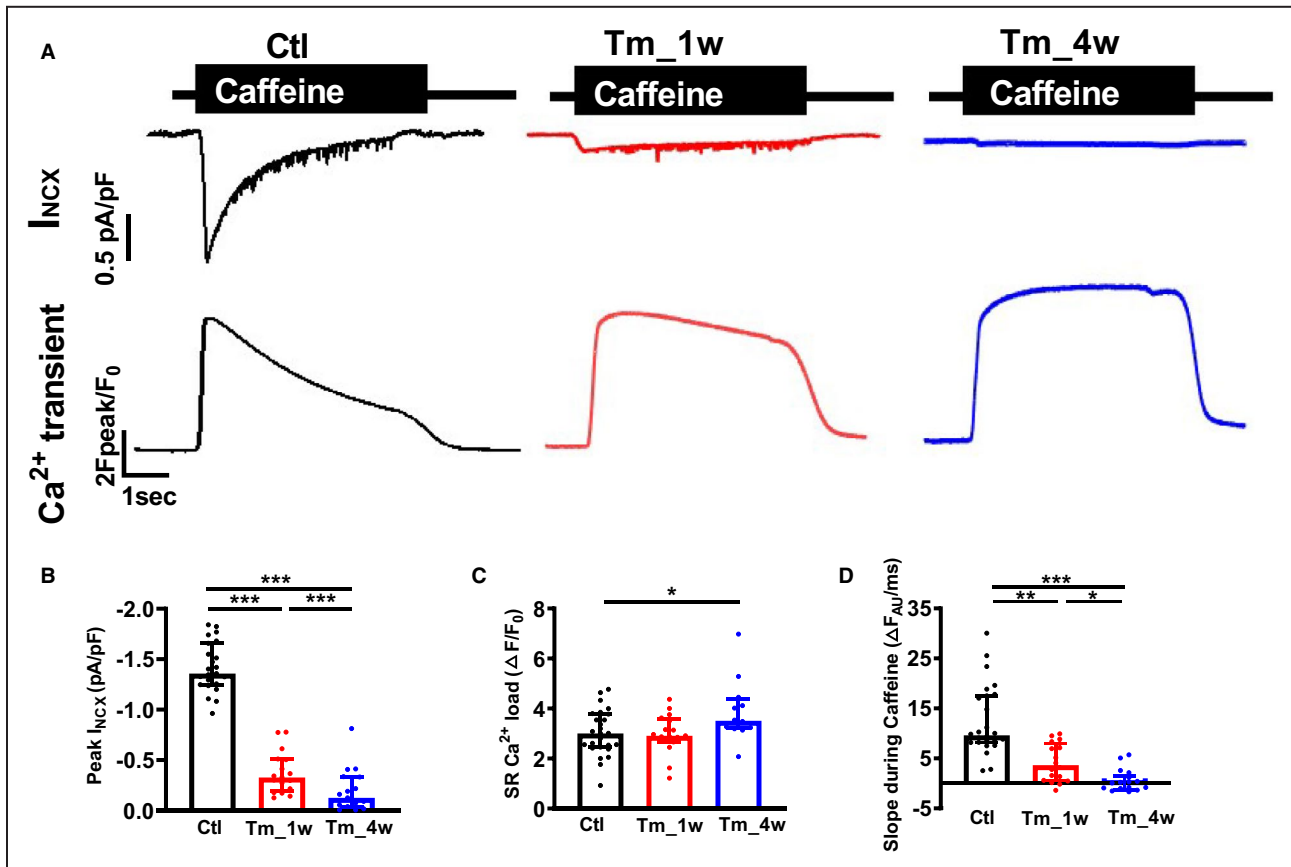


Figure 4. Sodium-calcium (Ca^{2+}) exchanger (NCX) isoform 1 (NCX1) current and sarcoplasmic reticulum (SR) Ca^{2+} load in tamoxifen-inducible NCX1 knockout (KO) mice.

A, Representative NCX current (I_{NCX} , top) and simultaneously recorded Ca^{2+} transient (bottom) from patch-clamped ventricular cardiomyocytes loaded with Fluo-4 in response to caffeine (10 mmol/L caffeine for 5 seconds) in control mice (Ctl) and tamoxifen-inducible NCX1 KO mice at 1 week (Tm_1w, red) and 4 weeks (Tm_4w, blue) post-tamoxifen. **B**, Summary data showing peak I_{NCX} and **(C)** mean SR Ca^{2+} release amplitude ($\Delta F/F_0$) induced by caffeine (reflecting SR Ca^{2+} load) and **(D)** mean slope of decline of the Ca^{2+} transient during caffeine perfusion (reflecting Ca^{2+} removal rates by NCX and plasma membrane calcium ATPase, and Ca^{2+} uptake by mitochondria). Data are expressed as median and interquartile range. Control mice (Ctl, N=25 cells from 5 mice) and mice 1 week (Tm_1w, N=18 cells from 4 mice) and 4 weeks (Tm_4w, N=19 cells from 3 mice) after tamoxifen injection. * P <0.05, ** P <0.01, *** P <0.001 by Kruskal-Wallis test.

subsarcolemmal Ca^{2+} , undetectable by conventional methods, was responsible.³¹

Since Fluo-4 is a nonratiometric indicator, subject to artifacts caused by differences in dye loading, bleaching, and cell thickness, it cannot be used to reliably assess diastolic Ca^{2+} between cells. To accurately determine whether elevations in diastolic Ca^{2+} were occurring in tamoxifen NCX1 KO mice, we used the ratiometric Ca^{2+} indicator Fura-2 to measure Ca^{2+} transient ratios (F_{360}/F_{390}) in field-stimulated myocytes (1 Hz) using the custom-designed dual excitation/single-emission epifluorescence detection system described above.³² We observed a substantial increase of diastolic Fura-2 fluorescence ratios at 1 week post-tamoxifen (control $3.2 \pm 0.1 F_{360/390}$ [N=90] and 1 week $3.6 \pm 0.1 F_{360/390}$ [N=62]; P <0.01) and increased systolic

Ca^{2+} as well (control $4.1 \pm 0.1 F_{360/390}$ and 1 week $4.7 \pm 0.1 F_{360/390}$; P <0.001), although these levels returned to baseline at 4 weeks (Figure 6). Notably, the 4-week time point coincides with the increase in SR Ca^{2+} load (Figure 4C).

We observed increased SERCA2 and PMCA4 protein expression (Figure 6C) in the NCX1 KO mice. The increased ratio of SERCA2 to phospholamban suggests an increase in SR Ca^{2+} pumping ability. Thus, as the NCX1 protein decreases in tamoxifen-injected NCX1 KO mice, there is increased expression of SR Ca^{2+} uptake proteins and alternative sarcolemmal Ca^{2+} efflux proteins. In addition, we observed an increase of the p-CaMKII/CaMKII ratio 1 week after tamoxifen injection, which has implications for the phosphorylation and function of several EC coupling proteins.

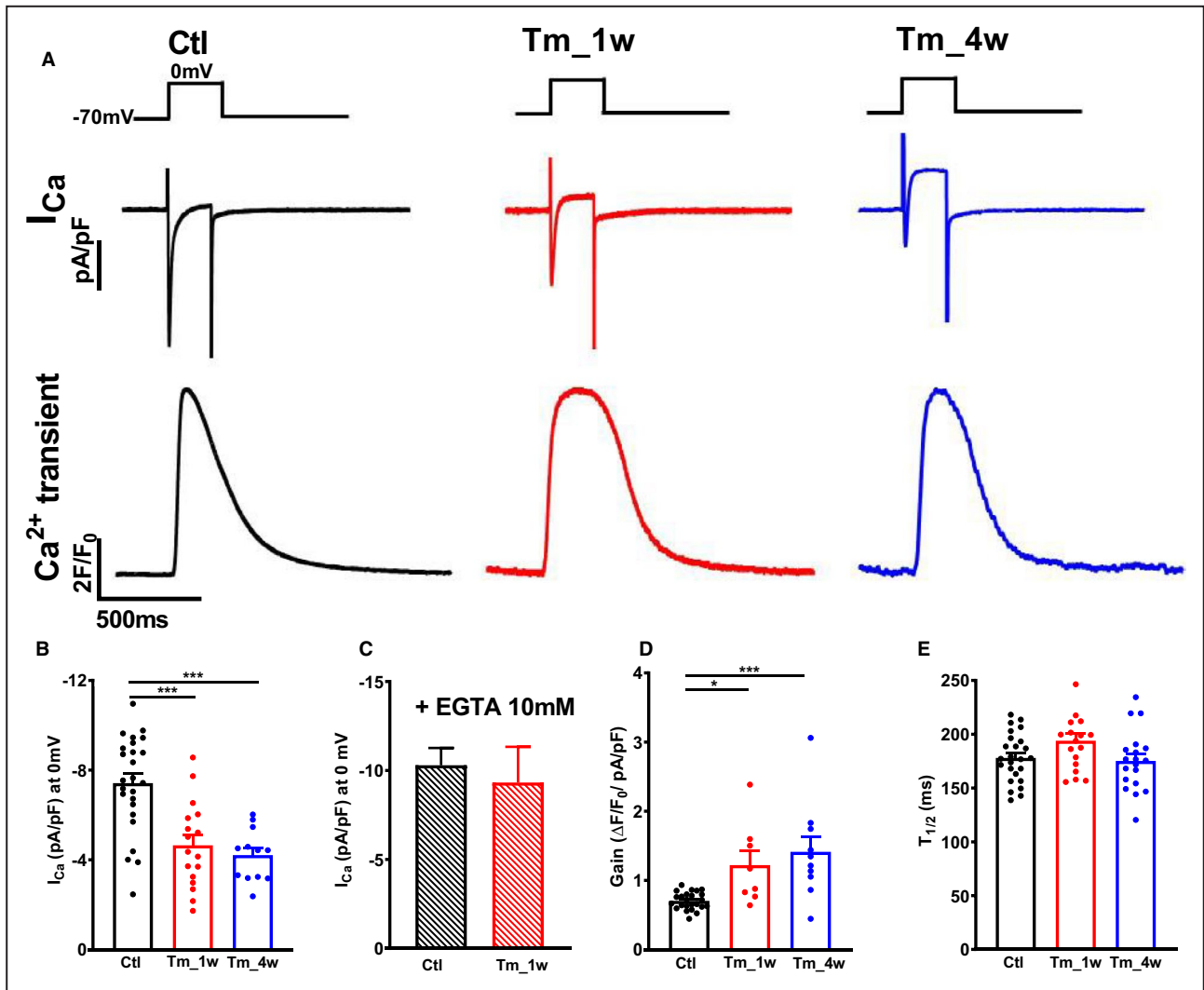


Figure 5. Excitation-contraction (EC) coupling in tamoxifen-inducible sodium-calcium (Ca^{2+}) exchanger isoform 1 (NCX1) knockout (KO) mice.

A, Representative voltage protocol (top), Ca^{2+} current (I_{Ca} , middle), and simultaneously recorded Ca^{2+} transient (bottom) in patch-clamped ventricular myocytes in control (Ctl) and tamoxifen-inducible NCX1 KO mice at 1 week (Tm_1w) and 4 weeks (Tm_4w) post-tamoxifen. **B**, Mean data showing I_{Ca} density (pA/pF) at 0 mV. **C**, Mean data showing I_{Ca} density (pA/pF) at 0 mV with EGTA (10 mmol/L) in the pipette. **D**, Mean data showing EC coupling gain ($\Delta F/F_0$ /pA/pF) at 0 mV. **E**, Mean data showing Ca^{2+} transient relaxation half-time ($T_{1/2}$, ms) in myocytes from control (Ctl) and tamoxifen-inducible NCX1 KO mice at 1 week (Tm_1w) and 4 weeks (Tm_4w) post-tamoxifen. Data are expressed as mean \pm SEM. Control mice (Ctl, N=25 cells from 5 mice) and mice 1 week (Tm_1w, N=17 cells from 4 mice) and 4 weeks (Tm_4w, N=12 cells from 3 mice) after tamoxifen injection. For EGTA experiments control mice (Ctl, N=8 cells from 2 mice) and mice 1 week after tamoxifen injection (Tm_1w, N=6 cells from 2 mice). * P <0.05, *** P <0.001. Statistics are calculated by 1-way ANOVA (**B**, **D**, and **E**) or Student t test (**C**).

AP Shortening in Tamoxifen-Inducible NCX1 KO Mice

Previous NCX KO mice (both ventricular and atrial-specific) feature shortened AP duration (APD). To determine the effect of acute ablation of NCX1 on APD, we recorded membrane voltage in control and NCX1 KO myocytes using the patch-clamp technique with the amplifier in bridge balance current-clamp mode. There was no change in resting membrane potential in KO myocytes (Figure 7A; control -67.8 ± 0.7 mV

[N=16], 1 week -67.3 ± 0.6 mV [N=17], and 4 weeks -67.6 ± 0.7 mV [N=19] [$P=0.86$]). At a stimulation rate of 0.5 Hz, there was a striking loss in the AP plateau (APD at 90% repolarization [APD90]) at 1 week, which was even more pronounced 4 weeks after tamoxifen (Figure 7A; control 41.5 ± 3.6 ms [N=16], 1 week 22.0 ± 2.4 ms [N=17] [$P=0.0139$], and 4 weeks 13.8 ± 1.2 ms [N=19] [$P<0.001$]). APDs at 10% repolarization [APD10] and 20% repolarization (APD20) were unchanged at 1 week but significantly shortened

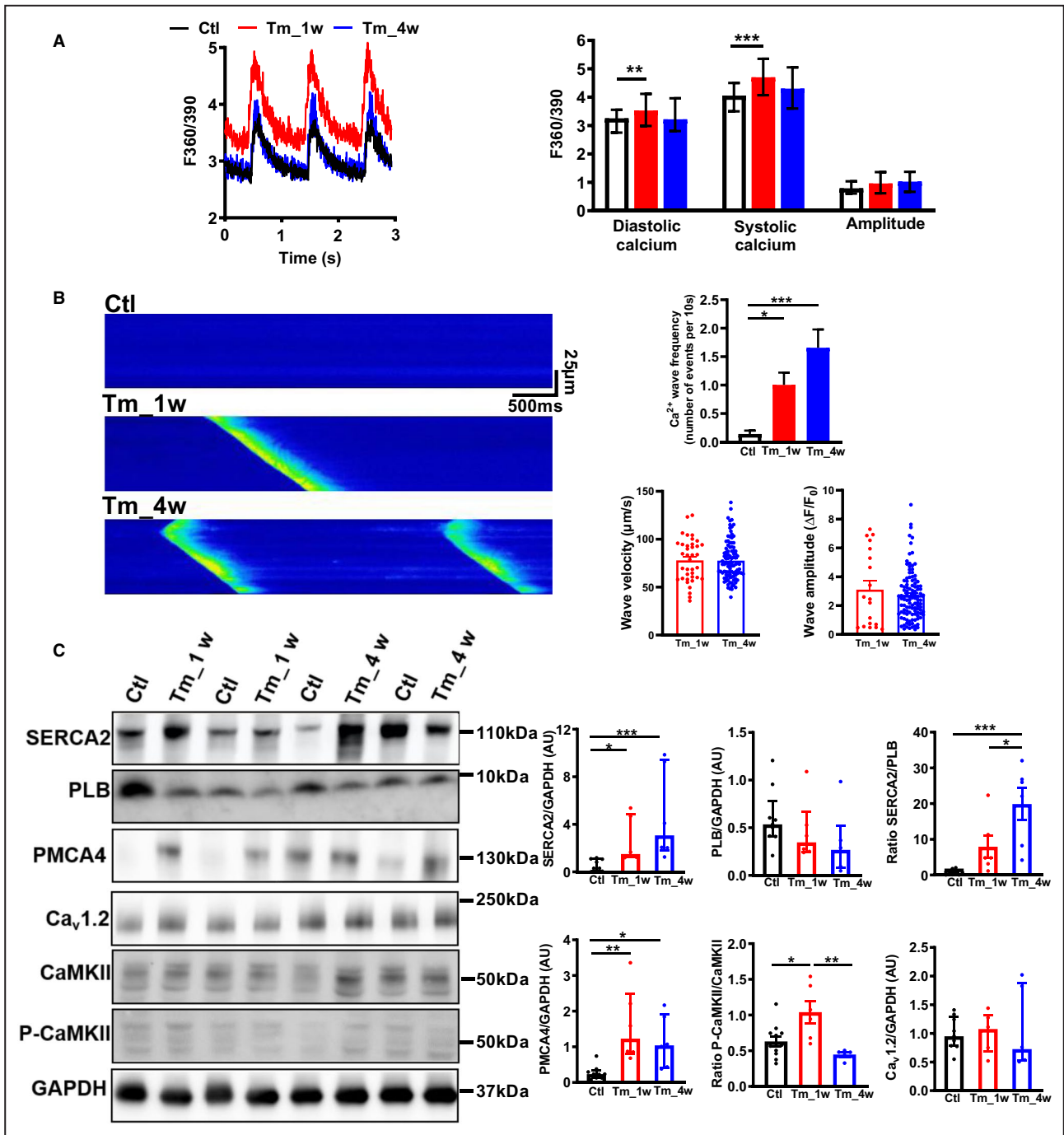
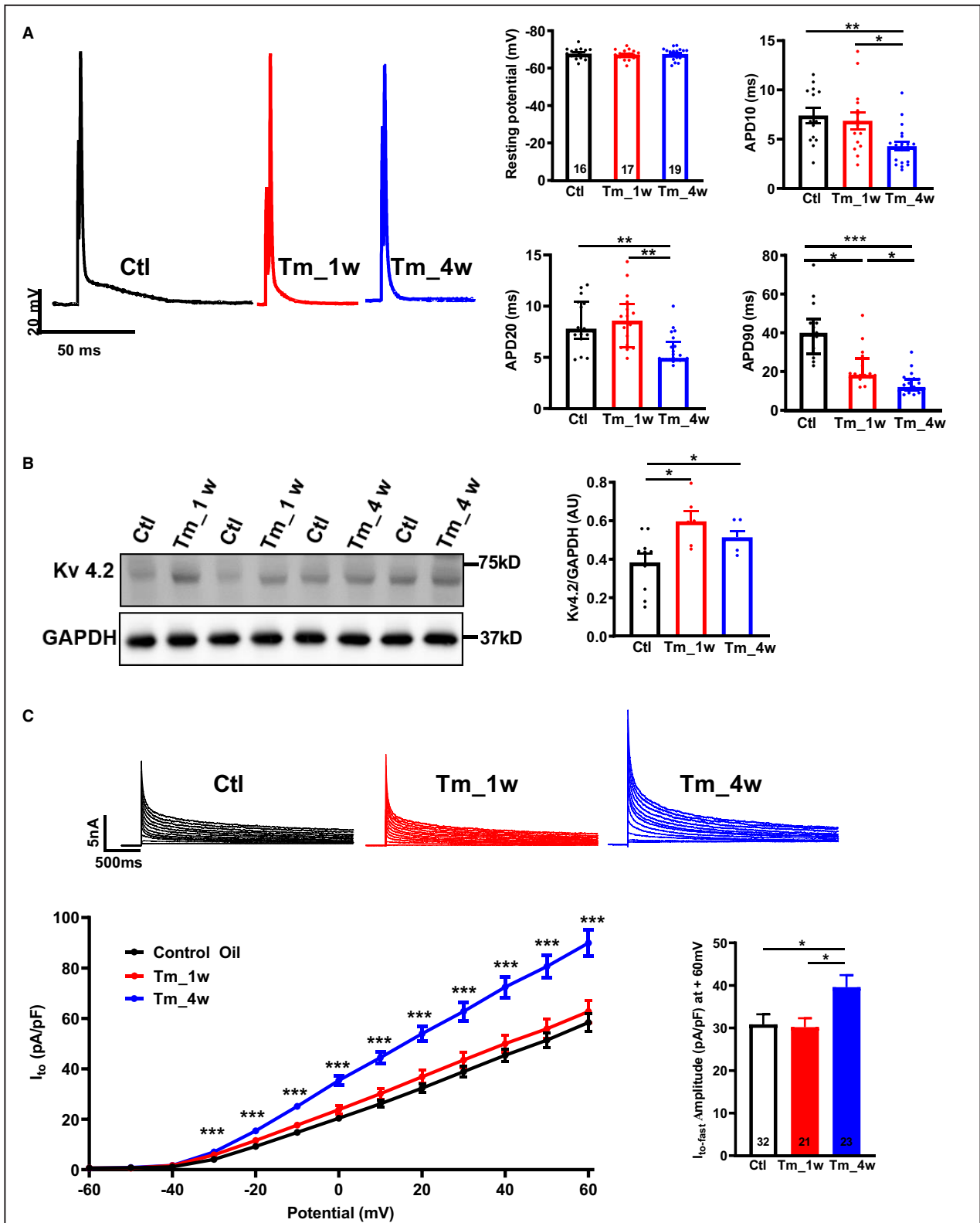


Figure 6. Adaptations of calcium (Ca²⁺) handling in tamoxifen-inducible sodium-Ca²⁺ exchanger isoform 1 (NCX1) knockout (KO) mice.

A, Representative traces (left) and summary data (right) of Ca²⁺ transients recorded using Fura-2 acetoxymethyl ester in control mice (Ctl, black) and tamoxifen-inducible NCX1 KO mice at 1 week (Tm_1w, red) and 4 weeks (Tm_4w, blue) post-tamoxifen. **B**, Representative confocal line scans (left) and summary data (right) of Ca²⁺ wave frequency, velocity (μm/s), and amplitude (ΔF/F₀) recorded in isolated ventricular myocytes loaded with Fluo-4 acetoxymethyl ester from control mice (Ctl, N=66 cells from 8 mice) and mice 1 week (Tm_1w, N=47 cells from 4 mice) and 4 weeks (Tm_4w, N=62 cells from 6 mice) after tamoxifen injection. **C**, Representative Western blots (left) and summary data (right) from ventricular cardiomyocytes showing sarcoplasmic reticulum Ca²⁺ ATPase 2 (SERCA2), phospholamban (PLB), plasma membrane calcium ATPase 4 (PMCA4), Ca_v1.2 (calcium channel voltage-dependent L type α 1C subunit), calcium/calmodulin-dependent protein kinase II (CaMKII), and phosphorylated CaMKII (P-CaMKII) expression. Mean data normalized to GAPDH. Data are expressed as mean±SEM (1-way ANOVA) or median and interquartile range (Kruskal-Wallis). Data from control mice (Ctl, N=9) and mice 1 week (Tm_1w, N=6) and 4 weeks (Tm_4w, N=6 mice) after tamoxifen injection. *P<0.05, **P<0.01, ***P<0.001 by 1-way ANOVA (p-CaMKII/CaMKII ratio, SERCA2/PLB ratio, wave frequency) or Kruskal-Wallis (F340/380, SERCA2/GAPDH, PMCA4/GAPDH, PLB/GAPDH, Ca_v1.2/GAPDH).



4 weeks post-tamoxifen (Figure 7A; APD10: control 7.4 ± 0.8 ms [N=16], 1 week 6.9 ± 0.8 ms [N=17], and 4 weeks 4.3 ± 0.4 ms [N=19] [$P < 0.01$]; APD20: control 8.3 ± 0.6 ms [N=16], 1 week 8.6 ± 0.7 ms [N=17], and

4 weeks 5.7 ± 0.3 ms [N=19] [$P < 0.01$]). In mouse myocardium, NCX has little effect on APD,^{17,33} contrary to species with longer APDs such as rabbit, human, and guinea pig.³⁴⁻³⁶ Thus, ablation of NCX, by itself,

Figure 7. Shortened action potential (AP) and transient outward potassium current (I_{to}) in ventricular cardiomyocytes from tamoxifen-inducible sodium-calcium exchanger isoform 1 (NCX1) knockout (KO) mice.

A, Representative APs recorded from patch-clamped ventricular myocytes (left), summary data showing resting potential (mV, middle), and AP duration (APD) at 10% repolarization (APD10), 20% repolarization (APD20), and 90% repolarization (APD90; right) in myocytes from control mice (Ctl, N=16 cells from 9 mice) and mice 1 week (Tm_1w, N=17 cells from 8 mice) and 4 weeks (Tm_4w, N=19 cells from 8 mice) after tamoxifen injection. **B**, Representative blots (left) and summary data (right) from ventricular cardiomyocytes showing Kv4.2 expression. Mean data are normalized to GAPDH. Control mice (Ctl, N=9) and mice 1 week (Tm_1w, N=6) and 4 weeks (Tm_4w, N=6) after tamoxifen injection. **C**, Representative traces of I_{to} (top), summary data comparing the current-voltage relationship for I_{to} (bottom left), and summary data comparing amplitude at +60 mV of the fast component of I_{to} ($I_{to\text{fast}}$) (bottom right) in myocytes from control mice (Ctl, N=32 cells from 8 mice) and mice 1 week (Tm_1w, N=21 cells from 4 mice) and 4 weeks (Tm_4w, N=23 cells from 6 mice) after tamoxifen injection. Data are expressed as mean \pm SEM (1-way ANOVA) or median and interquartile range (Kruskal-Wallis) from n=8 to 11 cells. * P <0.05, ** P <0.01, *** P <0.001 by Kruskal-Wallis test (APD90, APD20) or 1-way ANOVA.

seems unlikely to account for the reduction in APD90 that we observed. Other possibilities include a reduction in I_{Ca} ³⁷ and increases in repolarizing K^+ currents, as we have previously shown.^{15,17} Thus, we performed Western blots to evaluate the expression of the voltage-dependent K^+ channel subunit Kv4.2, a critical component of I_{to} . We observed a significant increase at 1 and 4 weeks post-tamoxifen injection (Figure 7B; control 0.38 ± 0.04 AU [N=9], 1 week 0.60 ± 0.05 AU [N=6], and 4 weeks 0.51 ± 0.03 AU [N=6] [$P=0.0105$]). Using the whole-cell patch-clamp technique, we then recorded I_{to} in control and NCX1 KO mice using our published protocol.¹⁷ Despite the increase in Kv4.2, there was no increase in I_{to} 1 week after tamoxifen (N=21), but there was a significant increase at 4 weeks (Figure 7C; $I_{to\text{fast}}$ +60 mV; control 30.9 ± 2.4 pA/pF [N=32] and 4 weeks 39.6 ± 2.8 pA/pF [N=23] [$P=0.0334$]). This corresponds with the reduction to APD10 and APD20 repolarization at 4 weeks, but does not explain the reduction in APD90 at 1 or 4 weeks.

sAPs and I/R Injury

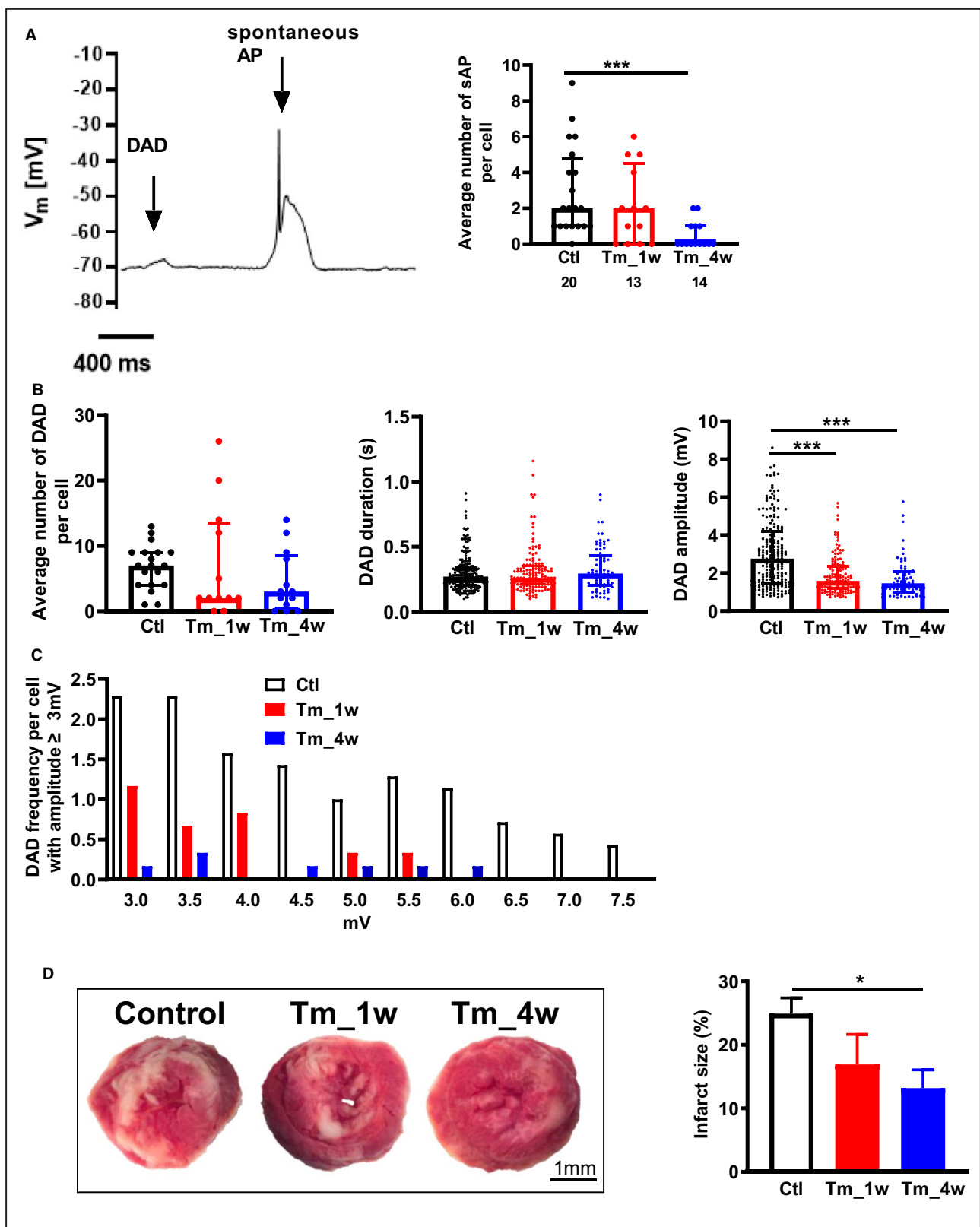
NCX1 is thought to facilitate arrhythmogenic delayed afterdepolarizations (DADs) in response to spontaneous release of SR Ca^{2+} .³⁸ To determine whether acute ablation of NCX1 is protective against DADs and DAD-induced sAPs, we applied a proarrhythmic stimulation protocol³⁹ in isolated cardiomyocytes from control and tamoxifen-treated mice. We performed whole-cell patch-clamp with the Axopatch 900A amplifier and applied 20 stimulations at 5, 2, 1, 0.5, and 0.125 Hz, followed by 1 minute of rest. We defined DADs as clear depolarizations of low amplitude during diastole that did not induce an AP. sAPs were defined as APs that occurred in the absence of a current clamp command (Figure 8A). At 1 and 4 weeks post-tamoxifen injection, induced DADs occurred with the same frequency as controls. However there was a significant reduction in the average number of sAPs per cell (Figure 8A; control 3.0 ± 0.6 [N=7], 1 week 2.1 ± 0.6 [N=6], and 4 weeks 0.5 ± 0.2 by [N=6] [P <0.001]). The reduced incidence of sAPs corresponded with a reduction in the mean amplitude of

DADs (Figure 8B, right panel; mean DAD amplitude in mV: control 3.0 ± 0.1 [N=7], 1 week 1.9 ± 0.1 [N=6] [P <0.001], and 4 weeks 1.6 ± 0.1 [N=6] [P <0.001]). There was no change in DAD duration, which remained at the typical duration observed in other mouse studies.^{39,40} Closer examination revealed that sAPs corresponded with DADs exhibiting an amplitude >3 mV, which are extremely rare 4 weeks post-tamoxifen (Figure 8C). As mentioned earlier, 25% of cells at 4 weeks post-tamoxifen have no I_{NCX1} , similar to the 15% of cells at 4 weeks that have no DADs and no sAP. Since DADs are produced by spontaneous Ca^{2+} release, we used confocal imaging in Fluo-4-loaded ventricular myocytes to assess frequency and velocity of spontaneous Ca^{2+} waves at different time points after tamoxifen injection. Wave frequency was low in control cells, but significantly increased at 1 week and further increased at 4 weeks after tamoxifen (Figure 6B, right). There was no change in wave velocity at any time point (Figure 6B). Thus, tamoxifen-induced acute ablation of NCX1 can reduce DADs and arrhythmogenic sAPs despite an increase in spontaneous Ca^{2+} waves.

To examine whether NCX1 KO hearts are protected from I/R injury, we subjected Langendorff-perfused hearts to zero-flow global ischemia followed by 2 hours of reperfusion. Infarct size was significantly smaller in the NCX1 hearts subjected to I/R 4 weeks post-tamoxifen injection (Figure 8D; control $24.9\pm 2.5\%$ [N=8], 1 week $16.9\pm 4.7\%$ [N=3], and 4 weeks $13.2\pm 2.9\%$ [N=6] [$P=0.0268$]) consistent with the hypothesis that reverse-mode Na^+/Ca^{2+} exchange contributes to IR injury, a finding we also observed in the MLC2v NCX1 KO mouse model.²⁴

DISCUSSION

We previously generated a ventricular-specific NCX1 KO mouse using Cre/loxP technology and the MLC2v promoter. Adaptations of EC coupling physiology in that chronic NCX1 ablation model permitted these mice to live to reproductive age. However, extensive remodeling characterized by fibrosis and ventricular hypertrophy, associated with a reduction



in ejection fraction, was evident as the animals aged. Furthermore, these mice had a reduced lifespan and were difficult to breed because of reduced tolerance to pregnancy. In the present study, we created mice

with tamoxifen-inducible ablation of NCX1 function to avoid these limitations. NCX1 protein expression in whole ventricular tissue homogenate, which contains only 49.2% of ventricular cardiomyocytes,⁴¹ is barely

Figure 8. Cardioprotective effects of cardiac sodium-calcium exchanger (NCX1) ablation in arrhythmia and ischemia/reperfusion (I/R) injury.

A, Representative delayed after depolarization (DAD) and spontaneous action potential (AP) in a patch-clamped myocyte under current-clamp mode and mean data showing the average number of spontaneous APs per cell recorded over 3.9 minutes. **B**, Mean data showing the average number of DADs per cell over 3.9 minutes, DAD duration (s), and DAD amplitude (mV) in myocytes from control mice (Ctl, N=7) and tamoxifen-inducible NCX isoform 1 (NCX1) knockout (KO) mice at 1 week (Tm_1w, N=6) and 4 weeks (Tm_4w, N=6) post-tamoxifen injection. **C**, Frequency distribution of individual DADs with amplitude ≥ 3 mV in all investigated cells in myocytes from control mice (N=7) and tamoxifen-inducible NCX1 KO mice 1 week (N=6) and 4 weeks (N=6) post-tamoxifen injection. **D**, Representative cross-sectional images of control and tamoxifen-inducible NCX1 KO hearts following I/R incubated with 2,3,5-triphenyltetrazolium chloride (left), and mean data of infarct size in the percentage measured at 120 minutes of reperfusion (right). Data are expressed as mean \pm SEM (1-way ANOVA) or median and interquartile range (Kruskal-Wallis) from n=13 to 20 cells for DAD experiments and N=3 to 8 hearts for I/R experiments. V_m indicates membrane potential. * $P < 0.05$, *** $P < 0.001$ by 1-way ANOVA (infarct size) or Kruskal-Wallis test.

detectable within 1 week of tamoxifen injection and even further decreased by 4 weeks. At the cellular level, the percentage of residual I_{NCX} is slightly higher because nonmyocytes are not included in the average. Nevertheless, 25% of cardiomyocytes exhibit no I_{NCX} whatsoever. This is likely a consequence of <100% efficiency of MerCreMer¹⁸ and the Cre/lox method in general.¹⁴ A major advantage of this model is that ablation of NCX1 can be induced at any age, and the mice breed readily. When compared with the MLC2v NCX1 KO model, tamoxifen-inducible NCX1 KO mice use an alternative set of adaptations to EC coupling and Ca^{2+} regulation. Nevertheless, these mice retain the characteristic cardioprotection from I/R injury and reduced burden of arrhythmogenic sAPs described in previous NCX KO models. This is a critical finding, as it confirms that the lack of NCX common to both models, and not the specific adaptations for survival, confers the beneficial effects. Similarly, our results suggest that the fibrosis and hypertrophy common to both models can be attributed to long-term NCX ablation.

Reduced Ca^{2+} Entry but Increased EC Coupling Gain in the Tamoxifen Mouse

Similar to our previous findings in the MLC2v NCX1 KO mouse,^{14–17} tamoxifen-inducible NCX1 KO mice exhibit a reduction in I_{Ca} caused by Ca^{2+} -dependent inactivation (Figure 5C). At 1 week, this is likely a consequence of the increased resting cytoplasmic Ca^{2+} we observed. We did not directly test the role of Ca^{2+} -dependent inactivation at 4 weeks when the increase in diastolic Ca^{2+} is no longer evident. However, we assume that the 4-week mouse is analogous to the MLC2v model, where nondetectable (by fluorescent indicator) elevated subsarcolemmal Ca^{2+} produces Ca^{2+} -dependent inactivation of I_{Ca} with attendant reductions in amplitude.¹⁶ Thus, we may conclude that reduction in Ca^{2+} entry through LCCs is a common mechanism of adaptation to the loss of NCX1, as it decreases the burden on remaining Ca^{2+} efflux mechanisms to maintain Ca^{2+} homeostasis. The other adaptation reducing Ca^{2+} influx is the shortened APD^{14,16,17} present as early as 1 week post-tamoxifen

(Figure 7A). We observed the same in the MLC2v NCX1 KO mouse, and determined that it was caused by increased I_{to} .¹⁷ However, the mechanism for APD shortening in the tamoxifen mouse is not clear. I_{to} was not increased at 1 week (Figure 7C) despite an increase in the I_{to} subunit $K_v4.2$. Furthermore, quantitative polymerase chain reaction analysis did not reveal any increase in transcription of other components of I_{to} or other repolarizing K^+ channels, including $K_v4.3$, $K_v4.2$, $K_v1.4$, and $Kir2.1$ (Figure S3). The combination of reduced inward current caused by near elimination of NCX and reduced I_{Ca} at 1 week (Figure 5) is an attractive explanation for APD90 shortening, but this degree of reduction does not shorten APD90 in mouse AP simulations.¹⁷ Ramos-Franco et al⁴² have shown APD shortening when pharmacological blockers of NCX are applied in intact perfused hearts, but the specificity of the blockers is uncertain. Further investigation to better understand these changes in APD are needed.

Although I_{Ca} is reduced in the KO model, Ca transients are not diminished, indicating an increase in EC coupling gain (Figure 5D). We also observed increased gain in the MLC2v NCX1 KO mice,¹⁶ and we assume the same mechanism is operating here: increased coupling fidelity between LCCs and RyRs facilitated by baseline elevation in dyadic cleft Ca^{2+} .³¹ Increased cleft Ca^{2+} improves the likelihood of RyR triggering by LCC openings, even when these openings are brief.⁴³ While the MLC2v and tamoxifen models both feature increased EC coupling gain, only the tamoxifen model has completely preserved LV systolic function (Figure 2A and 2B), consistent with a previous report by Gao et al.¹⁹ Since Ca^{2+} transients are preserved in both models, we speculate that it is the excess fibrosis in the MLC2v model⁴⁴ that impairs LV function, although changes in the response of myofilaments to Ca^{2+} cannot be excluded.

Ca^{2+} Removal Mechanisms and Relation to Spontaneous Ca^{2+} Waves

One of the main advantages of using a tamoxifen-inducible KO model is that we can induce NCX deletion in the adult mouse at any age. This allows assessment

of how mature ventricular myocytes adapt to the sudden loss of NCX, as compared with elimination of NCX during cardiac development in the MLC2v NCX1 KO model. Within 1 week of completing tamoxifen injections, we observed an increase of diastolic and systolic Ca^{2+} during field stimulation of isolated myocytes loaded with Fura-2 (Figure 6A). The increase in cytosolic Ca^{2+} occurred despite an increase in PMCA4 (Figure 6C), an alternative but relatively minor Ca^{2+} efflux mechanism, and coincided with an increase in spontaneous Ca^{2+} waves (Figure 6B). A similar degree of increase in diastolic Ca^{2+} was reported by Bourgonje et al⁴⁵ following perfusion of the NCX inhibitor SEA-0400 (1 $\mu\text{mol/L}$) in dog cardiomyocytes. Such increases in cytosolic Ca^{2+} are expected to increase RyR open probability and produce Ca^{2+} waves.⁴⁶ Waves may also occur as a consequence of the increased p-CaMKII/CaMKII ratio (Figure 6C), which induces RyR2-Ser2814 phosphorylation and RyR2-mediated Ca^{2+} leak.⁴⁷⁻⁴⁹ Ca^{2+} waves persisted/increased at 4 weeks, likely in response to the increase in SR Ca^{2+} load (Figure 4C), which can also provoke Ca^{2+} waves.⁵⁰ The increased ratio of p-CaMKII/CaMKII can also produce phosphorylation of phospholamban on the Thr¹⁷ site, thereby further activating SERCA2 and promoting the eventual restoration of normal diastolic Ca^{2+} ^{46,51} and increased SR Ca^{2+} load at 4 weeks post-tamoxifen. We did not check phospholamban phosphorylation, although the SERCA2/phospholamban ratio was considerably increased over 4 weeks (Figure 6C), favoring enhanced SERCA activity and increased SR Ca^{2+} uptake.

Temporal Changes in RNA Expression

We took advantage of RNA sequencing to further understand temporal changes in gene expression in response to ablation of NCX1. Within 1 week of completing tamoxifen injection, IPA analysis revealed that the most significant cardiac changes were in the transcriptomic network coding for Cardiovascular Enlargement and Disease. Within that network, the PPARGC1A gene was upregulated (Figure 3E). This gene encodes peroxisome proliferator-activated receptor- γ coactivator 1 α (PGC-1 α), a well-known transcriptional coactivator that regulates energy metabolism and especially mitochondrial biogenesis.^{52,53} It is tempting to speculate that the increase in diastolic Ca^{2+} observed at 1 week promotes expression and activation of PGC-1 α , whose expression can be modulated by calcineurin.⁵⁴ Notably, PGC-1 α activity may oppose maladaptive cardiac remodeling⁵⁴ and also upregulate SERCA2.⁵⁵ By 4 weeks post-tamoxifen, RNA sequencing revealed statistically significant activation of cardiac fibrosis and cardiovascular disease networks, featuring up-regulation of TGF β and several other profibrogenic

extracellular matrix genes including COL1a1 and COL3a1 (Figure 3F).⁵⁶⁻⁵⁸ These findings correspond to the cardiac remodeling we observed, i.e., increased heart weight/body weight ratio, fibrosis, and myocyte cross-sectional area (Figure 2). Changes of EC coupling gene expression (Figure 3F) did not correlate well with protein expression or function (Figure 6C). For example, while both phospholamban and CACNA1C were downregulated, we found no reduction in corresponding protein expression. In our MLC2v NCX1 KO mouse, we found no changes in EC coupling gene or protein expression.¹⁴

Role of NCX in Arrhythmia and I/R Injury

NCX has been implicated in the pathogenesis of I/R injury, heart failure, and arrhythmia.^{6,59-64} The inward current carried by NCX in response to spontaneous SR Ca^{2+} release is thought to be the cause of DADs,³⁸ the substrate for triggered arrhythmia.⁶⁵ Bögeholz et al³⁹ showed that early after depolarization and DAD amplitudes are reduced in heterozygous global NCX1 KO mice, with fewer triggered sAPs, consistent with this hypothesis. In the present study, we found that the incidence of sAPs was reduced 4 weeks after tamoxifen injection (Figure 8A), a point where I_{NCX} is absent in 25% of cells and negligible in the rest, despite increased occurrence of spontaneous Ca^{2+} waves (Figure 6B) and no change in the frequency of DADs overall (Figure 8B). The reduction in sAPs could, in part, be explained by the shortening of the AP and the increase of I_{to} .⁶⁶⁻⁶⁹ However, we favor a different explanation: a reduction in DAD amplitude. Although the average number of induced DADs was similar in control and NCX1 KO animals, DAD amplitude was decreased in the KO mice (Figure 8B and 8C), and most of these DADs did not reach the voltage threshold needed to induce arrhythmogenic sAPs. Four weeks after tamoxifen injection, I_{NCX1} was eliminated in 25% of the cells and 15% of the cells had no DADs whatsoever. Only 7% of NCX1 KO cells at 4 weeks had DADs >3 mV, compared with 44% of control cells. We conclude that NCX1 is essential to produce DADs of sufficient amplitude to trigger arrhythmogenic sAPs; in contrast, genetic reduction of NCX1 protects against them.

Several lines of evidence support the detrimental role of NCX1 during reperfusion after ischemia. Depression of oxidative metabolism and increased anaerobic glycolysis inhibit the Na^+/K^+ ATPase and generate protons, both of which elevate intracellular Na^+ .⁷⁰⁻⁷² The low pH inhibits NCX1 activity so that it cannot remove Na^+ . When pH normalizes upon reperfusion, NCX1 suddenly becomes active, and the ensuing reverse $\text{Na}^+/\text{Ca}^{2+}$ exchange in response to elevated Na^+ leads to a rapid and catastrophic influx

of Ca^{2+} , causing cell death. Consistent with this hypothesis, we previously found that the MLC2v NCX1 KO mouse was resistant to I/R injury.²⁴ In the current study, we found that the tamoxifen-inducible NCX1 KO mouse is also resistant to I/R (Figure 8D), confirming a contribution of NCX1 to I/R injury. Despite these cardioprotective features, these mice had reduced survival compared with control (Figure 2D). The mode of death is unknown, but we observed onset of lethargy a few days before death more consistent with heart failure than arrhythmia. Notably, the MLC2v NCX1 KO also has a high mortality, and telemetry in those animals did not show evidence of arrhythmic death.⁴⁴

CONCLUSIONS

The tamoxifen-inducible cardiac-specific NCX1 KO mouse retains the major benefits of NCX1 ablation we described in the MLC2v mouse, e.g., cardioprotection from I/R and reduced arrhythmogenic sAPs. In addition, this mouse has several advantages over the ventricular-specific MLC2v NCX1 KO mouse. The tamoxifen mouse is easy to breed, KO of NCX1 can be initiated at any age, and ventricular contractility remains preserved without excessive fibrosis and hypertrophy even 4 weeks after tamoxifen. Timed inducibility of NCX1 ablation also facilitates study of the time course of adaptations in Ca^{2+} handling, allowing us to assess relative effectiveness at regulating intracellular Ca^{2+} under the stress of progressive reduction in Ca^{2+} efflux. Similarly, we can follow the time course of gene expression in response to ablation of NCX1. Unlike pharmacological inhibitors of NCX, we can be confident that the tamoxifen-inducible mouse specifically ablates NCX1. Adaptations are a direct compensation for NCX1 ablation and not indicative of off-target or nonselective effects of gene manipulation. Thus, these mice can be used to directly and reliably test the specificity of NCX1 blockers. Any further changes in EC coupling and Ca^{2+} handling by a purported NCX blocker would be a clear indication of poor selectivity for NCX. Finally, the ease of breeding means that it is now possible to produce more complex genetic modifications through crosses with other genetically modified mice.

ARTICLE INFORMATION

Received December 21, 2020; accepted May 12, 2021.

Affiliations

Smidt Heart Institute, Cedars-Sinai Medical Center, Los Angeles, CA (S.L., R.Z., A.H., C.G., D.G., S.A., J.I.G.); Division of Molecular Medicine, Department of Anesthesiology and Perioperative Medicine (M.O.), and Department of Physiology (K.D.P.), David Geffen School of Medicine at UCLA, Los Angeles, CA.

Acknowledgments

The authors thank Cedars-Sinai Biobank and Translational Research Core, UCLA Technology Center for Genomics & Bioinformatics.

Sources of Funding

This work was supported by the National Institutes of Health RO1 HL048509 (Goldhaber and Philipson) and HL147569 (Goldhaber and Ottolia).

Disclosures

None.

Supplementary Material

Tables S1–S2

Figures S1–S3

REFERENCES

- Eisner D, Bode E, Venetucci L, Trafford A. Calcium flux balance in the heart. *J Mol Cell Cardiol*. 2013;58:110–117. DOI: 10.1016/j.yjmcc.2012.11.017.
- Bers DM. Cardiac excitation–contraction coupling. *Nature*. 2002;415:198–205. DOI: 10.1038/415198a.
- Bridge J, Smolley JR, Spitzer K. The relationship between charge movements associated with ICa and INa-Ca in cardiac myocytes. *Science*. 1990;248:376. DOI: 10.1126/science.2158147.
- Philipson KD, Nicoll DA. Sodium-calcium exchange: a molecular perspective. *Annu Rev Physiol*. 2000;62:111–133. DOI: 10.1146/annurev.physiol.62.1.111.
- Reuter H, Henderson SA, Han T, Ross RS, Goldhaber JI, Philipson KD. The $\text{Na}^+\text{-Ca}^{2+}$ exchanger is essential for the action of cardiac glycosides. *Circ Res*. 2002;90:305–308. DOI: 10.1161/hh0302.104562.
- Pott C, Eckardt L, Goldhaber JI. Triple threat: the $\text{Na}^+\text{-Ca}^{2+}$ exchanger in the pathophysiology of cardiac arrhythmia, ischemia and heart failure. *Curr Drug Targets*. 2011;12:737–747. DOI: 10.2174/138945011795378559.
- Tanaka H, Nishimaru K, Aikawa T, Hirayama W, Tanaka Y, Shigenobu K. Effect of SEA0400, a novel inhibitor of sodium-calcium exchanger, on myocardial ionic currents. *Br J Pharmacol*. 2002;135:1096–1100. DOI: 10.1038/sj.bjpp.0704574.
- Elias CL, Lukas A, Shurraw S, Scott J, Omelchenko A, Gross GJ, Hnatoiwich M, Hryshko LV. Inhibition of $\text{Na}^+\text{-Ca}^{2+}$ exchange by KB-R7943: transport mode selectivity and antiarrhythmic consequences. *Am J Physiol Heart Circ Physiol*. 2001;281:H1334–H1345. DOI: 10.1152/ajpheart.2001.281.3.H1334.
- Kohajda Z, Farkas-Morvay N, Jost N, Nagy N, Geramipour A, Horváth A, Varga RS, Hornyik T, Corici C, Acsai K, et al. The effect of a novel highly selective inhibitor of the sodium/calcium exchanger (NCX) on cardiac arrhythmias in in vitro and in vivo experiments. *PLoS One*. 2016;11:e0166041. DOI: 10.1371/journal.pone.0166041.
- Terracciano CM, Hancox JC. ORM-10103: a significant advance in sodium-calcium exchanger pharmacology? *Br J Pharmacol*. 2013;170:765–767. DOI: 10.1111/bph.12299.
- Cho CH, Kim SS, Jeong M, Lee CO, Shin HS. The $\text{Na}^+\text{-Ca}^{2+}$ exchanger is essential for embryonic heart development in mice. *Mol Cells*. 2000;10:712–722. DOI: 10.1007/s10059-000-0712-2.
- Koushik SV, Wang J, Rogers R, Moskopidhis D, Lambert NA, Creazzo TL, Conway SJ. Targeted inactivation of the sodium-calcium exchanger (Ncx1) results in the lack of a heartbeat and abnormal myofibrillar organization. *FASEB J*. 2001;15:1209–1211. DOI: 10.1096/fj.00-0696fje.
- Orban PC, Chui D, Marth JD. Tissue- and site-specific DNA recombination in transgenic mice. *Proc Natl Acad Sci USA*. 1992;89:6861–6865. DOI: 10.1073/pnas.89.15.6861.
- Henderson SA, Goldhaber JI, So JM, Han T, Motter C, Ngo A, Chantawansri C, Ritter MR, Friedlander M, Nicoll DA, et al. Functional adult myocardium in the absence of $\text{Na}^+\text{-Ca}^{2+}$ exchange. *Circ Res*. 2004;95:604–611. DOI: 10.1161/01.RES.0000142316.08250.68.
- Pott C, Henderson SA, Goldhaber JI, Philipson KD. $\text{Na}^+\text{-Ca}^{2+}$ Exchanger knockout mice. *Ann N Y Acad Sci*. 2007;1099:270–275. DOI: 10.1196/annals.1387.015.
- Pott C, Philipson KD, Goldhaber JI. Excitation-contraction coupling in $\text{Na}^+\text{-Ca}^{2+}$ exchanger knockout mice: reduced transsarcolemmal

- Ca²⁺ flux. *Circ Res*. 2005;97:1288–1295. DOI: 10.1161/01.RES.0000196563.84231.21.
17. Pott C, Ren X, Tran DX, Yang MJ, Henderson S, Jordan MC, Roos KP, Garfinkel A, Philipson KD, Goldhaber JL. Mechanism of shortened action potential duration in Na⁺-Ca²⁺ exchanger knockout mice. *Am J Physiol Cell Physiol*. 2007;292:C968–C973. DOI: 10.1152/ajpcell.00177.2006.
 18. Sohal DS, Nghiem M, Crackower MA, Witt SA, Kimball TR, Tymitz KM, Penninger JM, Molkenin JD. Temporally regulated and tissue-specific gene manipulations in the adult and embryonic heart using a tamoxifen-inducible Cre protein. *Circ Res*. 2001;89:20–25. DOI: 10.1161/hh1301.092687.
 19. Gao Z, Rasmussen TP, Li Y, Kutschke W, Koval OM, Wu Y, Wu Y, Hall DD, Joiner MLA, Wu XQ, et al. Genetic inhibition of Na⁺-Ca²⁺ exchanger current disables fight or flight sinoatrial node activity without affecting resting heart rate. *Circ Res*. 2013;112:309–317. DOI: 10.1161/CIRCRESAHA.111.300193.
 20. Schneider CA, Rasband WS, Eliceiri KW. NIH Image to ImageJ: 25 years of image analysis. *Nat Methods*. 2012;9:671–675. DOI: 10.1038/nmeth.2089.
 21. Robinson MD, McCarthy DJ, Smyth GK. edgeR: a Bioconductor package for differential expression analysis of digital gene expression data. *Bioinformatics*. 2010;26:139–140. DOI: 10.1093/bioinformatics/btp616.
 22. Fowler CJ, Tiger G. Calibration of Fura-2 signals introduces errors into measurement of thrombin-stimulated calcium mobilisation in human platelets. *Clin Chim Acta*. 1997;265:247–261. DOI: 10.1016/S0009-8981(97)00139-3.
 23. Yin L, Bien H, Entcheva E. Scaffold topography alters intracellular calcium dynamics in cultured cardiomyocyte networks. *Am J Physiol Heart Circ Physiol*. 2004;287:H1276–H1285. DOI: 10.1152/ajpheart.01120.2003.
 24. Imahashi K, Pott C, Goldhaber Joshua I, Steenbergen C, Philipson Kenneth D, Murphy E. Cardiac-specific ablation of the Na⁺-Ca²⁺ exchanger confers protection against ischemia/reperfusion injury. *Circ Res*. 2005;97:916–921. DOI: 10.1161/01.RES.0000187456.06162.cb.
 25. Redfors B, Shao Y, Omerovic E. Myocardial infarct size and area at risk assessment in mice. *Exp Clin Cardiol*. 2012;17:268–272.
 26. Han Y, Gao S, Muegge K, Zhang W, Zhou B. Advanced applications of RNA sequencing and challenges. *Bioinform Biol Insights*. 2015;9:29–46. DOI: 10.4137/BBIS.52891.
 27. Hrdlickova R, Toloue M, Tian B. RNA-Seq methods for transcriptome analysis. *Wiley Interdiscip Rev RNA*. 2017;8:e1364. DOI: 10.1002/wrna.1364.
 28. Fukumoto GH, Lamp ST, Motter C, Bridge JH, Garfinkel A, Goldhaber JL. Metabolic inhibition alters subcellular calcium release patterns in rat ventricular myocytes. *Circ Res*. 2005;96:551–557. DOI: 10.1161/01.RES.0000159388.61313.47.
 29. Goldhaber JL, Parker JM, Weiss JN. Mechanisms of excitation-contraction coupling failure during metabolic inhibition in guinea-pig ventricular myocytes. *J Physiol*. 1991;443:371–386. DOI: 10.1113/jphysiol.1991.sp018838.
 30. Goldhaber JL. Free radicals enhance Na⁺/Ca²⁺ exchange in ventricular myocytes. *Am J Physiol*. 1996;271:H823–H833. DOI: 10.1152/ajpheart.1996.271.3.H823.
 31. Pott C, Yip M, Goldhaber JL, Philipson KD. Regulation of cardiac L-type Ca²⁺ current in Na⁺-Ca²⁺ exchanger knockout mice: functional coupling of the Ca²⁺ channel and the Na⁺-Ca²⁺ exchanger. *Biophys J*. 2007;92:1431–1437. DOI: 10.1529/biophysj.106.091538.
 32. Kilfoil PJ, Lotteau S, Zhang R, Yue X, Aynaszyan S, Solymani RE, Cingolani E, Marban E, Goldhaber JL. Distinct features of calcium handling and β -adrenergic sensitivity in heart failure with preserved versus reduced ejection fraction. *J Physiol*. 2020;598:5091–5108. DOI: 10.1113/JP280425.
 33. Bondarenko VE, Szigeti GP, Bett GCL, Kim S-J, Rasmusson RL. Computer model of action potential of mouse ventricular myocytes. *Am J Physiol Heart Circ Physiol*. 2004;287:H1378–H1403. DOI: 10.1152/ajpheart.00185.2003.
 34. Spencer CI, Sham JS. Effects of Na⁺/Ca²⁺ exchange induced by SR Ca²⁺ release on action potentials and afterdepolarizations in guinea pig ventricular myocytes. *Am J Physiol Heart Circ Physiol*. 2003;285:H2552–H2562. DOI: 10.1152/ajpheart.00274.2003.
 35. Bers DM. Species differences and the role of sodium-calcium exchange in cardiac muscle relaxation. *Ann N Y Acad Sci*. 1991;639:375–385. DOI: 10.1111/j.1749-6632.1991.tb17326.x.
 36. Noble D, Noble SJ, Bett GC, Earm YE, Ho WK, So IK. The role of sodium–calcium exchange during the cardiac action potential. *Ann N Y Acad Sci*. 1991;639:334–353. DOI: 10.1111/j.1749-6632.1991.tb17323.x.
 37. Song LS, Guia A, Muth JN, Rubio M, Wang SQ, Xiao RP, Josephson IR, Lakatta EG, Schwartz A, Cheng H. Ca²⁺ signaling in cardiac myocytes overexpressing the α 1 subunit of L-type Ca²⁺ channel. *Circ Res*. 2002;90:174–181. DOI: 10.1161/hh0202.103230.
 38. Sipido KR, Bito V, Antoons G, Volders PG, Vos MA. Na/Ca exchange and cardiac ventricular arrhythmias. *Ann N Y Acad Sci*. 2007;1099:339–348. DOI: 10.1196/annals.1387.066.
 39. Bögeholz N, Pauls P, Bauer BK, Schulte JS, Decherer DG, Frommeyer G, Kirchhefer U, Goldhaber JL, Müller FU, Eckardt L, et al. Suppression of early and late afterdepolarizations by heterozygous knockout of the Na⁺/Ca²⁺ exchanger in a murine model. *Circ Arrhythm Electrophysiol*. 2015;8:1210–1218. DOI: 10.1161/CIRCEP.115.002927.
 40. Ko CY, Liu MB, Song Z, Qu Z, Weiss JN. Multiscale determinants of delayed afterdepolarization amplitude in cardiac tissue. *Biophys J*. 2017;112:1949–1961. DOI: 10.1016/j.bpj.2017.03.006.
 41. Litviňuková M, Talavera-López C, Maatz H, Reichart D, Worth CL, Lindberg EL, Kanda M, Polanski K, Heinig M, Lee M, et al. Cells of the adult human heart. *Nature*. 2020;588:466–472. DOI: 10.1038/s41586-020-2797-4.
 42. Ramos-Franco J, Aguilar-Sanchez Y, Escobar AL. Intact heart loose patch photolysis reveals ionic current kinetics during ventricular action potentials. *Circ Res*. 2016;118:203–215. DOI: 10.1161/CIRCRESAHA.115.307399.
 43. Goldhaber JL, Philipson KD. Cardiac sodium-calcium exchange and efficient excitation-contraction coupling: implications for heart disease. *Adv Exp Med Biol*. 2013;961:355–364. DOI: 10.1007/978-1-4614-4756-6_30.
 44. Jordan MC, Henderson SA, Han T, Fishbein MC, Philipson KD, Roos KP. Myocardial function with reduced expression of the sodium-calcium exchanger. *J Card Fail*. 2010;16:786–796. DOI: 10.1016/j.cardfail.2010.03.012.
 45. Bourgonje VJ, Vos MA, Ozdemir S, Doisne N, Acsai K, Varro A, Sztojok-Ivanov A, Zupko I, Rauch E, Kattner L, et al. Combined Na⁺/Ca²⁺ exchanger and L-type calcium channel block as a potential strategy to suppress arrhythmias and maintain ventricular function. *Circ Arrhythm Electrophysiol*. 2013;6:371–379. DOI: 10.1161/CIRCEP.113.000322.
 46. Eisner DA, Caldwell JL, Kistamás K, Trafford AW. Calcium and excitation-contraction coupling in the heart. *Circ Res*. 2017;121:181–195. DOI: 10.1161/CIRCRESAHA.117.310230.
 47. Uchinoumi H, Yang Y, Oda T, Li N, Alsina KM, Puglisi JL, Chen-lzu Y, Cornea RL, Wehrens XH, Bers DM. CaMKII-dependent phosphorylation of RyR2 promotes targetable pathological RyR2 conformational shift. *J Mol Cell Cardiol*. 2016;98:62–72. DOI: 10.1016/j.yjmcc.2016.06.007.
 48. Ai X, Curran JW, Shannon TR, Bers DM, Pogwizd SM. Ca²⁺/calmodulin-dependent protein kinase modulates cardiac ryanodine receptor phosphorylation and sarcoplasmic reticulum Ca²⁺ leak in heart failure. *Circ Res*. 2005;97:1314–1322. DOI: 10.1161/01.RES.0000194329.41863.89.
 49. Curran J, Brown KH, Santiago DJ, Pogwizd S, Bers DM, Shannon TR. Spontaneous Ca waves in ventricular myocytes from failing hearts depend on Ca²⁺-calmodulin-dependent protein kinase II. *J Mol Cell Cardiol*. 2010;49:25–32. DOI: 10.1016/j.yjmcc.2010.03.013.
 50. Lukyanenko V, Subramanian S, Gyorke I, Wiesner TF, Gyorke S. The role of luminal Ca²⁺ in the generation of Ca²⁺ waves in rat ventricular myocytes. *J Physiol*. 1999;518:173–186. DOI: 10.1111/j.1469-7793.1999.0173r.x.
 51. Cheng H, Lederer MR, Lederer WJ, Cannell MB. Calcium sparks and [Ca²⁺]_i waves in cardiac myocytes. *Am J Physiol Cell Physiol*. 1996;270:C148–C159. DOI: 10.1152/ajpcell.1996.270.1.C148.
 52. Arany Z, He H, Lin J, Hoyer K, Handschin C, Toka O, Ahmad F, Matsui T, Chin S, Wu P-H, et al. Transcriptional coactivator PGC-1 α controls the energy state and contractile function of cardiac muscle. *Cell Metab*. 2005;1:259–271. DOI: 10.1016/j.cmet.2005.03.002.
 53. Finck BN, Kelly DP. PGC-1 coactivators: inducible regulators of energy metabolism in health and disease. *J Clin Invest*. 2006;116:615–622. DOI: 10.1172/JCI27794.
 54. Rowe GC, Jiang A, Arany Z. PGC-1 coactivators in cardiac development and disease. *Circ Res*. 2010;107:825–838. DOI: 10.1161/CIRCRESAHA.110.223818.
 55. Chen M, Wang Y, Qu A. PGC-1 α accelerates cytosolic Ca²⁺ clearance without disturbing Ca²⁺ homeostasis in cardiac myocytes. *Biochem Biophys Res Commun*. 2010;396:894–900. DOI: 10.1016/j.bbrc.2010.05.018.

56. Mukherjee S, Kolb MR, Duan F, Janssen LJ. Transforming growth factor- β evokes Ca^{2+} waves and enhances gene expression in human pulmonary fibroblasts. *Am J Respir Cell Mol Biol*. 2012;46:757–764. DOI: 10.1165/rcmb.2011-0223OC.
57. Bhandary B, Meng Q, James J, Osinska H, Gulick J, Valiente-Alandi I, Sargent MA, Bhuiyan MS, Blaxall BC, Molkentin JD, et al. Cardiac fibrosis in proteotoxic cardiac disease is dependent upon myofibroblast TGF- β signaling. *J Am Heart Assoc*. 2018;7:e010013. DOI: 10.1161/JAHA.118.010013.
58. Khalil H, Kanisicak O, Prasad V, Correll RN, Fu X, Schips T, Vagnozzi RJ, Liu R, Huynh T, Lee SJ, et al. Fibroblast-specific TGF- β -Smad2/3 signaling underlies cardiac fibrosis. *J Clin Invest*. 2017;127:3770–3783. DOI: 10.1172/JCI94753.
59. Sipido KR, Volders PGA, Vos MA, Verdonck F. Altered Na/Ca exchange activity in cardiac hypertrophy and heart failure: a new target for therapy? *Cardiovasc Res*. 2002;53:782–805. DOI: 10.1016/S0008-6363(01)00470-9.
60. Bers DM, Pogwizd SM, Schlotthauer K. Upregulated Na/Ca exchange is involved in both contractile dysfunction and arrhythmogenesis in heart failure. *Basic Res Cardiol*. 2002;97:136–142. DOI: 10.1007/s003950200027.
61. Pogwizd SM, Bers DM. Cellular basis of triggered arrhythmias in heart failure. *Trends Cardiovasc Med*. 2004;14:61–66. DOI: 10.1016/j.tcm.2003.12.002.
62. Pogwizd SM, Qi M, Yuan W, Samarel AM, Bers DM. Upregulation of $\text{Na}^+/\text{Ca}^{2+}$ exchanger expression and function in an arrhythmogenic rabbit model of heart failure. *Circ Res*. 1999;85:1009–1019. DOI: 10.1161/01.res.85.11.1009.
63. Pott C, Muszynski A, Ruhe M, Bögeholz N, Schulte JS, Milberg P, Mönning G, Fabritz L, Goldhaber JI, Breithardt G, et al. Proarrhythmia in a non-failing murine model of cardiac-specific $\text{Na}^+/\text{Ca}^{2+}$ exchanger overexpression: whole heart and cellular mechanisms. *Basic Res Cardiol*. 2012;107:247. DOI: 10.1007/s00395-012-0247-7.
64. Sipido KR, Volders PG, de Groot SH, Verdonck F, Van de Werf F, Wellens HJ, Vos MA. Enhanced Ca^{2+} release and Na/Ca Exchange activity in hypertrophied canine ventricular myocytes. *Circulation*. 2000;102:2137–2144. DOI: 10.1161/01.cir.102.17.2137.
65. Marban E, Robinson SW, Wier WG. Mechanisms of arrhythmogenic delayed and early afterdepolarizations in ferret ventricular muscle. *J Clin Invest*. 1986;78:1185–1192. DOI: 10.1172/JCI112701.
66. Workman AJ, Marshall GE, Rankin AC, Smith GL, Dempster J. Transient outward K^+ current reduction prolongs action potentials and promotes afterdepolarisations: a dynamic-clamp study in human and rabbit cardiac atrial myocytes. *J Physiol*. 2012;590:4289–4305. DOI: 10.1113/jphysiol.2012.235986.
67. Kuo HC, Cheng CF, Clark RB, Lin JC, Lin JC, Hoshijima M, Nguyễn-Trần VT, Gu Y, Ikeda Y, Chu PH, et al. A defect in the Kv channel-interacting protein 2 (KChIP2) gene leads to a complete loss of I_{to} and confers susceptibility to ventricular tachycardia. *Cell*. 2001;107:801–813. DOI: 10.1016/S0092-8674(01)00588-8.
68. London B, Baker LC, Petkova-Kirova P, Nerbonne JM, Choi BR, Salama G. Dispersion of repolarization and refractoriness are determinants of arrhythmia phenotype in transgenic mice with long QT. *J Physiol*. 2007;578:115–129. DOI: 10.1113/jphysiol.2006.122622.
69. Huang CL. Murine electrophysiological models of cardiac arrhythmogenesis. *Physiol Rev*. 2017;97:283–409. DOI: 10.1152/physrev.00007.2016.
70. Steenbergen C, Deleew G, Rich T, Williamson JR. Effects of acidosis and ischemia on contractility and intracellular pH of rat heart. *Circ Res*. 1977;41:849–858. DOI: 10.1161/01.RES.41.6.849.
71. Crampin EJ, Smith NP, Langham AE, Clayton RH, Orchard CH. Acidosis in models of cardiac ventricular myocytes. *Philos Trans A Math Phys Eng Sci*. 2006;364:1171–1186. DOI: 10.1098/rsta.2006.1763.
72. Orchard CH, Cingolani HE. Acidosis and arrhythmias in cardiac muscle. *Cardiovasc Res*. 1994;28:1312–1319. DOI: 10.1093/cvr/28.9.1312.

SUPPLEMENTAL MATERIAL

Table S1. Echocardiography Parameters.

	Control (N=9)			NCX1 KO (N=17)		
	Control	Ctl 1_w	Ctl 4_w	Tamoxifen	Tm_1w	Tam_4w
Age (week)	12.2±0.7	12.9±0.7	16.1±0.5	11.7±0.5	12.7±0.5	17.1±0.6
Heart rate (beats/min)	446±18	463±9	463±13	447±11	439±14	464±14
End diastolic dimension (mm)	3.81±0.09	4.00±0.09	4.01±0.05	3.93±0.06	4.13±0.06	3.85±0.12
End systolic dimension (mm)	2.56±0.10	2.76±0.11	2.90±0.11	2.67±0.07	2.94±0.07	2.68±0.12
Left ventricular ejection fraction (%)	61.7±2.7	58.9±2.2	57.6±3.6	60.9±1.6	57.6±1.7	57.5±2.7
Left ventricular fractional shortening (%)	32.9±1.8	30.9±1.5	28.1±3.0	32.4±1.2	29.2±1.4	30.0±1.8
Left ventricular diastolic anterior wall (mm)	0.89±0.05	0.81±0.06	0.87±0.07	0.81±0.06	0.89±0.04	1.04±0.06
Left ventricular systolic anterior wall (mm)	1.36±0.08	1.22±0.07	1.27±0.11	1.40±0.05	1.29±0.04	1.53±0.05
Left ventricular diastolic posterior wall (mm)	0.83±0.04	0.84±0.03	0.82±0.04	0.89±0.04	0.89±0.04	1.11±0.08*
Left ventricular systolic posterior wall (mm)	1.13±0.04	1.14±0.04	1.16±0.05	1.20±0.04	1.19±0.05	1.33±0.08

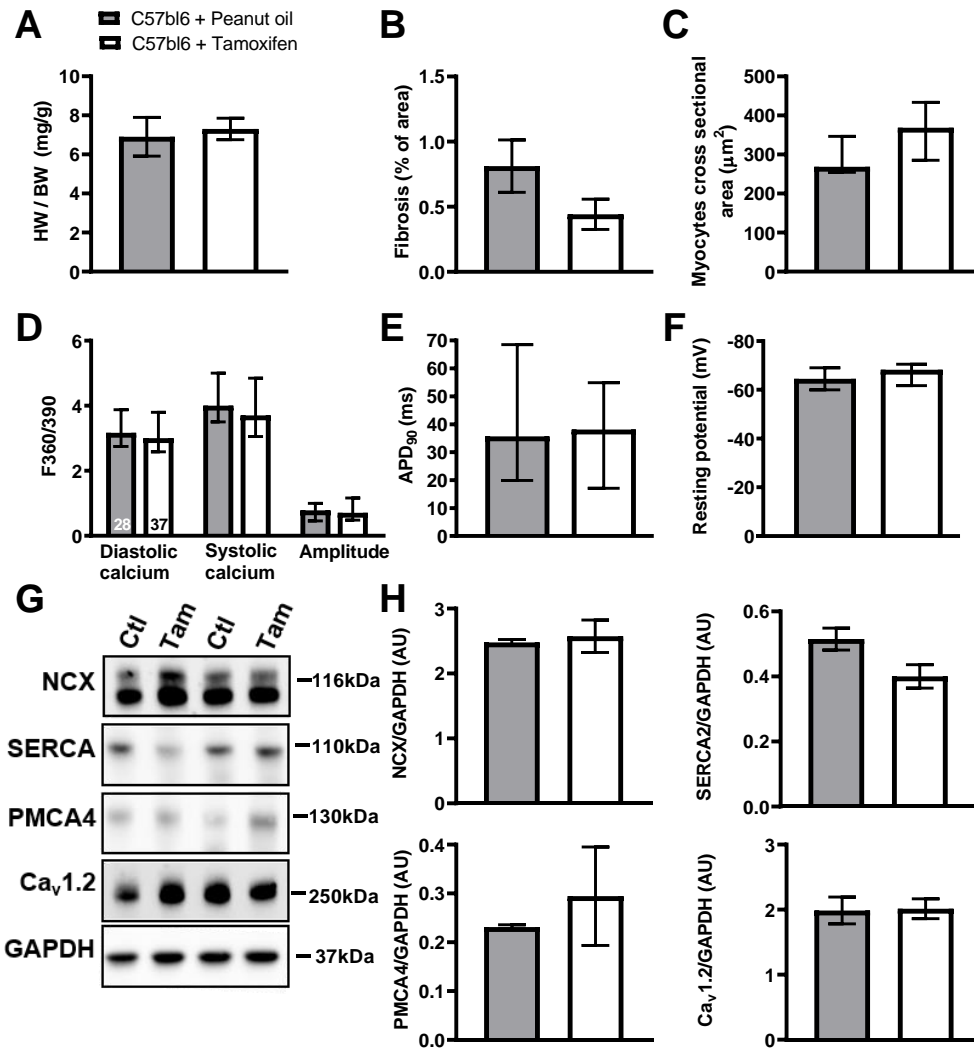
There are no changes in echo-derived parameters in the NCX1 KO mice at either 1 week (Tm_1w) or 4 weeks (Tm_4w) post tamoxifen. Data are expressed as mean ± SEM from N=9 control, N=17 NCX1 KO. *P<0.05 as compared with baseline from the same group by ANOVA.

Table S2. Network analysis table.

Top functions				
Tm_1w		Tm_4w		
5 total networks	Genes in network	25 total networks	Genes in network	
1	Cardiac Enlargement, Cardiovascular Disease, Cardiovascular System Development and Function	Acot1,ADRB1,AKT1,ANKRD1,BAD,CASP3,CAT,GDF15,HEY2,HK2,HMOX1,IGF1,IGF1R,IRF5,IRS2,KLF15,LDHB,Mcpt4,MEF2A,MLYCD,MYC,NPPA,Nppb,PDK4,PLIN5,Pln,PPARA,PPARGC1A,PRKCB,SIRT6,SLC18A3,SOD1,SOD2,TP53,UCP3	Energy Production, Lipid Metabolism, Small Molecule Biochemistry	ACAA2,ACADM,ACADVL,ACO2,ACOT2,ACOX1,ACSL1,ATP5F1B,Cox8b,CPT1B,CPT2,CRAT,CS,DECR1,ECI1,ETFA,ETFB,FH,FLNC,HADHA,HADHB,HSD17B10,INSR,KCNJ11,KLF15,MLYCD,OGDH,PLIN5,PNPLA2,PPARA,PPARGC1A,SLC25A20,Tpm2,UCP2,UCP3
2	Cellular Assembly and Organization, Cellular Development, Cellular Growth and Proliferation	ACTA1,ACTA2,ACTC1,AQP4,MEF2A,NR4A1	Cardiac Fibrosis, Cardiovascular Disease, Organismal Injury and Abnormalities	ACTA1,ADAMTS4,AGTR1,ANGPT1,APLN,CACNA1C,CAMK2A,CAV3,CCL11,COL1A1,COL3A1,CYBB,FOS,GPX3,HAND2,HMOX1,MAPK11,MB,MITF,MYH6,MYH7,NCF1,NPPA,Nppb,PCSK6,Pln,PRKCB,Retnla,RGS19,SLC2A4,SPTLC2,TGFB3,TNNI3,TNNT2,XDH
3	Embryonic Development, Organismal	MYCN,SMAD4	Cellular Movement, Hematological System Development and Function, Immune Cell Trafficking	ADORA2B,C5AR1,CASP3,Ccl2,CD14,CD44,CD80,CD86,COL8A1,CXCL2,EGFR,FN1,HEY1,HK2,HSPD1,IGF1,IL1B,IL1R1,IL1RN,IRAK4,MAP3K5,MMP2,NCF2,OLR1,PIK3CG,POSTN,PRKCD,PRKCE,PTN,RYR2,SDC1,SELP,SPARC,SPP1,TLR4
4	Cardiovascular Disease, Congenital Heart	Foxp1,MIR17HG,SOX4	Cell Death and Survival, Cell Morphology, Cell Signaling	ALDH4A1,ATG10,BAK1,CASP1,DBT,GSTM5,IER3,MYLK3,MYO1E,PANK1,PK2,SUCLG2,TCAP,TP53,TPM3,Tpm4,VCAN
5	Metabolic Disease, Organismal Injury and Abnormalities, Renal and Urological Disease	CTNNB1,NOS3,PTGS2	Cardiac Enlargement, Organismal Development, Organismal Injury and Abnormalities	ACTB,ADAM12,E2F1,EEF1A1,EPAS1,GRK5,HGF,IDH2,IRF5,MYH9,MYL3,NDUFS1,PFKFB1,PFKM,TNFRSF1A,TNFRSF1B,TP53

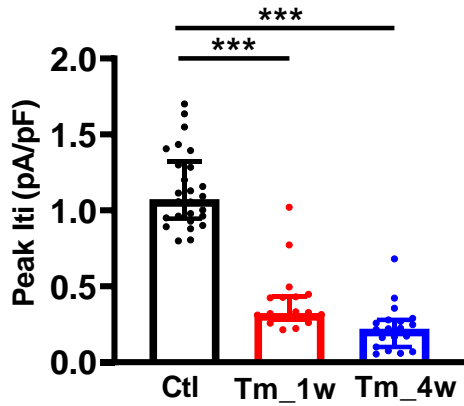
5 out of 5 major networks identified 1 week after tamoxifen injection (Tm_1w) showing genes in each involved network (*left*). 5 out of 25 networks identified 4 weeks after tamoxifen injection (Tm_4w) showing genes in each involved network (*right*).

Figure S1. Tamoxifen effects are absent in C57bl6 control mice.



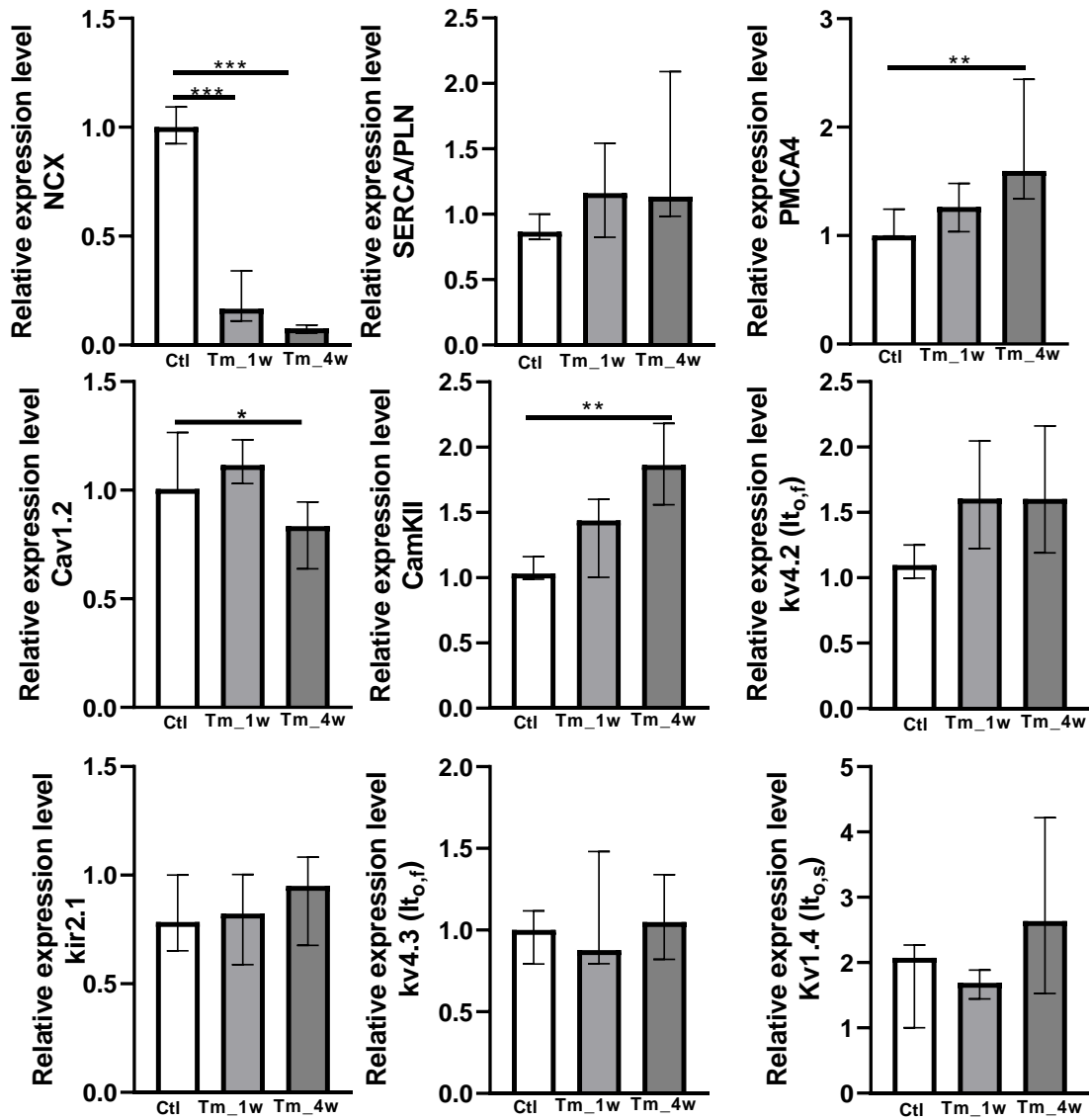
A. Summary data of heart weight to body weight ratios (HW/BW), **B.** fibrosis (% of total area), **C.** myocyte cross sectional area (μm^2), **D.** Ca^{2+} transient measured using fura-2 AM (F_{360/390}), **E.** action potential duration at 90% of repolarization (APD₉₀, in ms), **F.** resting potential (mV) in C57Bl6 mice injected with vehicle only (peanut oil, grey) or tamoxifen (white). **G.** Representative blots and **H.** summary data from ventricular cardiomyocytes showing NCX, SERCA2, PMCA4 and Ca_v1.2 expression. Mean data are normalized to GAPDH. Data are expressed as median and interquartile range from n=2 mice per condition by Mann-Whitney test.

Figure S2. Transient inward current upon repolarization (I_{ti}) reduced in NCX1 KO mice.



Summary data showing peak I_{ti} (pA/pF) in control (Ctl, N=25 cells from 5 mice), 1 week after tamoxifen injection (Tm_1w, N=17 cells from 4 mice), 4 weeks after tamoxifen injection (Tm_4w, N=12 cells from 3 mice). Data are expressed as median and interquartile range. *** $P < 0.001$, by Kruskal-Wallis test.

Figure S3. qPCR showing mRNA expression in Tamoxifen inducible NCX1 KO mice.



Mean data are normalized to GAPDH. Data are expressed as median and interquartile range from n=6 mice per condition. * P<0.01, by Kruskal-Wallis test.